Structural and Biochemical Analysis of HutD from *Pseudomonas fluorescens* SBW25

Yunhao Liu

A thesis submitted in fulfilment of the requirements for the degree of Master of Science in Molecular Biosciences at Massey University, Auckland, New Zealand

April 2008 – April 2009

Abstract

Pseudomonas fluorescens SBW25 is a gram-negative soil bacterium capable of growing on histidine as the sole source of carbon and nitrogen. Expression of histidine utilization (*hut*) genes is controlled by the HutC repressor with urocanate, the first intermediate of the histidine degradation pathway, as the direct inducer. Recent genome sequencing of *P. fluorescens* SBW25 revealed the presence of *hutD* in the *hut* locus, which encodes a highly conserved hypothetical protein. Previous genetic analysis showed that *hutD* is involved in *hut* regulation, in such a way that it prevents overproduction of the *hut* enzymes. Deletion of *hutD* resulted in a slow growth phenotype in minimal medium with histidine as the sole carbon and nitrogen source. While the genetic evidence supporting a role of *hutD* in *hut* regulation is strong, nothing is known of the mechanism of HutD action.

Here I have cloned and expressed the *P. fluorescens* SBW25 *hutD* in *E. coli*. Purified HutD was subjected to chemical and structural analysis. Analytic size-exclusion chromatography indicated that HutD forms a dimer in the elution buffer. The crystal structure of HutD was solved at 1.80 Å (R = 19.3% and R_{free} = 22.3%) by using molecular replacement based on HutD from *P. aeruginosa* PAO1. *P. fluorescens* SBW25 HutD has two molecules in an asymmetric unit and each monomer consists of one subdomain and two β-barrel domains. Comparative structural analysis revealed a conserved binding pocket. The interaction of formate with a highly conserved residue Arg61 via salt-bridges in the pocket suggests HutD binds to small molecules with carboxylic group(s) such as histidine, urocanate or formyl-glutamate.

The hypothesis that HutD functions via binding to urocanate, the *hut* inducer, was tested. Experiments using a thermal shift assay and isothermal titration calorimetry (ITC) analysis suggested that HutD binds to urocanate but not to histidine. However, the signal of HutD-urocanate binding was very weak and detected only at high urocanate concentration (53.23 mM), which is not physiologically relevant. The current data thus does not support the hypothesis of HutD-urocanate binding *in vivo*. Although the HutD-urocanate binding was not confirmed, this work has laid a solid foundation for further testing of the many alternative hypotheses regarding HutD function.

Acknowledgements

I am grateful to have worked with so many great people in a happy lab environment. First and foremost I would like to thank my supervisors Dr Xue-Xian Zhang and Professor Paul B. Rainey for all their time, advice, continued support and encouragement throughout the study. Thank you for providing such an interesting project to work on. Thanks to Dr. Jonathan C. Gauntlett for his help with protein purification. Thanks to Dr Wayne Patrick for his help with solubility and storage of the protein. To Dr Monica Gerth for all time and suggestions on writing this thesis. Thanks to all the students and staff in the Rainey lab who are always willing to help me.

I would also like to thank a number of people at the University of Auckland for their great help. Thanks to Dr. Ivan Ivanovich for all his help with the protein crystallization. To Dr. Shaun Lott and Dr. Jodie Margaret Johnston, I gratefully acknowledge the invaluable time spent helping me solve the protein structure, and all the advice on structural and biochemical studies. Thanks to Chen Gao for showing me the ropes when I first arrived at the Structural Biology Laboratory.

Lastly I would like to thank my parents for their encouragement, unconditional love and support.

Table of Contents

Abstract……..……ii
Acknowledgements……...iii
Table of Contents…….……iv
List of Figures……..vii
List of Tables……..……viii
List of Abbreviations…….……ix
Introduction……...……1
1.1 Histidine Degradation Pathway…….……1
1.2 Organization of *hut* operon…….……3
1.3 Regulation of histidine utilization (*hut*) genes…….……4
1.4 The role of HutD in histidine utilization……5
1.5 The 'governor' model of HutD action……...……7
1.6 Deducing protein function from structural information…….……8
1.7 Objectives of this study……..……8
Materials and Methods……...9
2.1 Reagents…….…9
2.2 Bioinformatics……9
2.2.1 Nucleotide and protein information……..9
2.2.2 Sequence homology search and alignment……...9
2.3 Bacterial strains, plasmids and growth conditions…….9
2.4 DNA manipulation……...10
2.4.1 Primer design……...10
2.4.2 Polymerase chain reaction……...11
2.4.3 DNA transformation……12
2.4.4 Preparation of electrocompetent *E. coli* cells……..12
2.4.5 Glycerol-saline stock……...12
2.4.6 Electroporation.……...13

2.4.7 Preparation of plasmid DNA……...13
2.4.8 Restriction enzyme digestion……...……...13
2.4.9 Agarose gel electrophoresis……13
2.4.10 DNA purification……...14
2.4.11 DNA ligation……14
2.5 Protein expression and solubility tests……14
2.5.1 Small-scale protein expression……14
2.5.2 Large-scale protein expression……14
2.5.3 Cell lysis and protein solubility tests……...15
2.6 Sodium Dodecyl Sulfate-PolyAcrylamide Gel Electrophoresis……..15
2.6.1 Gel preparation……15
2.6.2 Sample preparation, gel running and staining……16
2.7 Purification of hexa-histidine-tagged hutD……..17
2.8 Concentration of protein and buffer exchange……17
2.9 Size exclusion chromatography……....17
2.10 Determination of protein concentration……18
2.10.1 Determination of protein concentration by Bradford assay……..18
2.10.1 Determination of protein concentration by Beer-Lambert equation….18
2.11 Protein function tests……..19
2.11.1 Thermal shift assay……19
2.11.2 Isothermal titration calorimetry……19
2.12 Protein crystallization.……20
2.12.1 Initial crystallization trials……20
2.12.2 Optimization of crystallization conditions……21
2.13 Protein diffraction data collection……..21
2.13.1 Cryoprotectant test……21
2.13.2 Flash freezing crystals……...21
2.13.3 X-ray diffraction data collection……...22
2.14 Diffraction data processing……....22
2.14.1 Indexing, integration and scaling of diffraction data…….....22
2.14.2 Unit cell content analysis…….....22
2.14.3 Phase determination using molecular replacement…….....23
2.14.4 Model building and refinement……23

2.15 Structural analysis…….....23
Results…….24
3.1 Cloning of *hutD* to the expression vector pTrc99A…….24
3.2 Protein expression and purification…….....26
3.2.1 Small-scale expression and solubility of HutD……...26
3.2.2 Large-scale expression and purification of HutD……...30
3.3 Analytical size-exclusion chromatography…….....31
3.4 Crystallization of HutD……...33
3.4.1 Initial crystallization trials…….....33
3.4.2 Crystal optimization…….....33
3.5 Structure solution of HutD……...…35
3.5.1 Diffraction data collection and processing…….....35
3.5.2 Number of molecules in the asymmetric unit…….35
3.5.3 Phase determination by molecular replacement……..35
3.5.4 Model building, refinement and quality assessment…….....35
3.6 Description of HutD structure…….....40
3.6.1 Overall topology of HutD structure…….....40
3.6.2 Structural comparison of HutD monomer…….....41
3.7 Protein functional tests…….....45
3.7.1 Thermal shift assay……..46
3.7.2 Isothermal titration calorimetry……...49
Discussion……....52
4.1 The effect of growing temperature on HutD expression…….....52
4.2 Determination of molecular weight of HutD……52
4.3 Comparative structural analysis of HutD…….52
4.4 Function of HutD…….....54
Conclusion and Future Studies…….56
References……58

List of Figures

Figure 1.1 The histidine degradation pathway……2

Figure 1.2 Genetic and transcriptional organization of *hut* genes in *Pseudomonas* species……....4

Figure 1.3 Multiple sequence alignment of HutD sequence homologues……...6

Figure 1.4. Relative fitness of Δ*hutC* Δ*hutD* and Δ*hutCD* mutants……....…7

Figure 3.1 The map of pTrc99A expression vector…….....24

Figure 3.2 Construction of HutD expression plasmid pTrc99A-*hutD*……...25

Figure 3.3 Restriction digestion of pTrc99A-*hutD*…….....26

Figure 3.4 SDS-PAGE analysis of HutD expression at 37ºC……27

Figure 3.5 SDS-PAGE analysis of the solubility of HutD expressed at 37ºC……...28

Figure 3.6 SDS-PAGE analysis of HutD expression at 25ºC…….....29

Figure 3.7 SDS-PAGE analysis of the solubility of HutD expressed at 25ºC.....29

Figure 3.8 Purification of His_6-HutD by Ni-NTA affinity chromatography.....30

Figure 3.9 Gel filtration analysis of HutD…….……..…...……32

Figure 3.10 Initial crystallization of HutD……...33

Figure 3.11 Optimization of crystallization conditions…….....34

Figure 3.12 Ramachandran plot for the final model of HutD……..38

Figure 3.13 Cartoon representation of HutD dimer…….....40

Figure 3.14 Cartoon representation and topology diagram of HutD monomer.....41

Figure 3.15 Conservation pattern obtained using ConSurf for HutD…….…….....43

Figure 3.16 Conservation pattern obtained using ConSurf for HutD in *Pseudomonas*....44

Figure 3.17 Cartoon representation of putative binding pocket…….....…45

Figure 3.18 Recording of fluorescence internsity for different concentrations of HutD..46

Figure 3.19 Analysis of interaction of HutD with histidine and urocanate.....48

Figure 3.20 Isothermal titration calorimetry of histidine and HutD…….....50

Figure 3.21 Isothermal titration calorimetry of urocanate and HutD…….....51

List of Tables

Table 2.1 Bacterial strains and plasmids used in this study……...10

Table 2.2 Primers used in this study……..10

Table 2.3 Reagents for a 50 µl PCR reaction…….11

Table 2.4 Typical PCR reaction conditions…….……...11

Table 3.1 A summary of processing statistics of HutD crystal……..36

Table 3.2 Summary of refinement and model statistics…….....39

Table 3.3 Structural similarity of HutD monomer found using Dali and SSM……41

List of Abbreviations

Å	angstorms
ºC	degrees Celsius
µl	microlitre
µM	micromolar
APS	ammonium persulphate
BLAST	basic local alignment search tool
bp	base pairs
Da	Dalton
DNase	deoxyribonuclease I
dNTP	deoxynucleotide triphosphate
EDTA	ethylenediamine tetraacetic acid
g	gravitational force
h	hour
HEPES	n-2-hydroxylethylpiperazine-n'-2-ethanesulphonic acid
IPTG	isopropyl-β-D-thiogalactoside
ITC	isothermal titration calorimetry
kb	kilobase pairs
kDa	kiloDaltons
LB	luria-bertaini
LLG	log likelihood gain
M	molar
mg	milligram
ml	millimetre
min	minute
mM	millimolar
MR	molecular replacement
MW	molecular weight
MWCO	molecular weight cut-off
nm	nanometre
OD	optical density
ORF	open reading frames

PAGE	polyacrylamide gel electrophoresis
PCR	polymerase chain reaction
PISA	Protein Interfaces, Surfaces and Assemblies
PDB	Protein Data Bank
PMSF	phenylmethylsulfonyl fluoride
RNase	ribonuclease A
rpm	revolution per minute
SCOP	Structural Classification of Proteins
SEC	size exclusion chromatography
SDS	sodium dodecyl sulphate
SSM	Secondary Structure Matching
TAE	tris-acetate-EDTA
TEMED	N,N,N',N'-Tetramethylethylenediamine
TFZ	translation function Z-score
UV	ultraviolet

Introduction

1.1 Histidine degradation pathway

Pseudomonas fluorescens SBW25 is a metabolically versatile saprophytic soil bacterium that was originally isolated from the rhizosphere of field grown sugar beet (Thompson et al. 1995). Like enteric bacteria and other *Pseudomonas* strains, *P. fluorescens* SBW25 can grow on histidine as the sole source of carbon, nitrogen and energy. When growing in the plant environment, expression of genes involved in histidine utilization (*hut*) is elevated implicating an important role of histidine for bacterial colonization *in planta* (Zhang *et al*. 2006).

In bacteria, histidine is degradated via either a four- or a five-step enzymatic pathway with glutamate and ammonium as the end products (Figure 1.1). The two pathways have the first three steps in common from histidine to urocanate, to imidazolone propionate (IPA), to formiminoglutamate (FIGLU), which are catalyzed by histidase (HutH), urocanase (HutU) and imidazolone propionase (HutI), respectively. Breakdown of FIGLU to glutamate is mediated by a single enzyme (Itoh et al., 2007) in the four-step pathway, but two enzymes in the five-step pathway (FIGLU iminohydrolase encoded by *hutF* and formylglutamase encoded by *hutG*). Notably, an additional ammonium is produced in the five-step pathway. Excess ammonium is a stress that bacteria have to challenge mainly because it sends a nitrogen-replete signal causing the cessation of many catabolic enzymes including the *hut* enzymes.

It has been established that some enteric bacteria, such as *Salmonella typhimurium* (Magasanik, 1963), *Klebsiella aerogenes* (Lund and Magasanik, 1965) and the Gram-positive bacterium *Bacillus subtilis* (Chasin and Magasanik, 1968) employ the four-step histidine degradation pathway, whereas *Pseudomonas putida* (Hu et al., 1987) and *Streptomyces coelicolor* (Kendrick and Wheelis, 1982) use the five-step pathway. Genome sequencing and genetic characterization of *hutF* showed that *P. fluorescens* uses the five-step *hut* pathway (Zhang and Rainey, 2007).

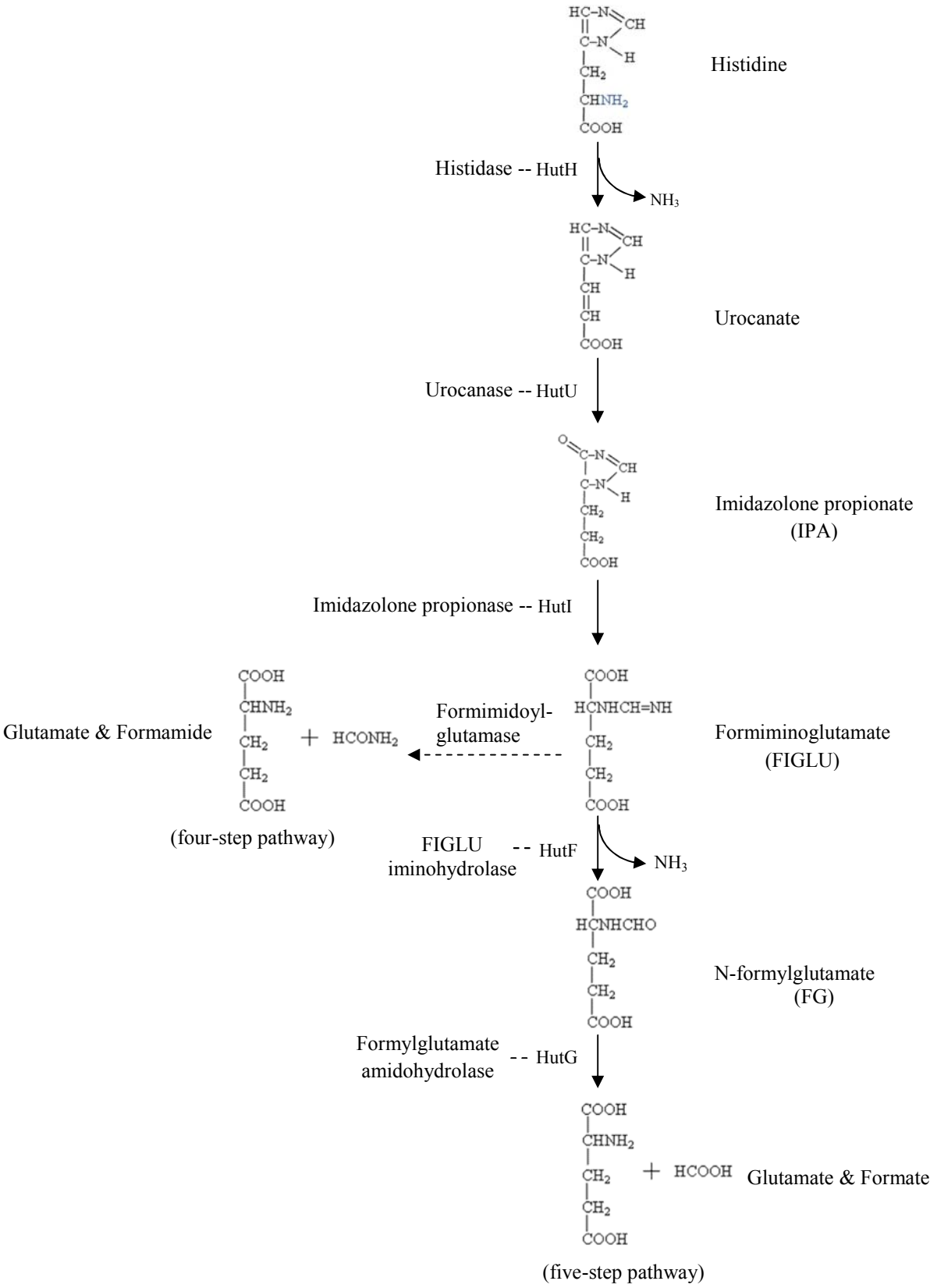

Figure 1.1. The histidine degradation pathway. Gene products involved in the degradation of histidine are: HutH--histidase; HutU--urocanase; HutI--imidazolone propionase; HutF--formiminoglutamate iminohydrolase; HutG--formylglutamate amidohydrolase.

1.2 Organization of *hut* operon

The *hut* genes in *P. fluorescens* SBW25 are organized in three transcriptional units (Figure 1.2). All the enzymatic genes, except *hutF*, together with putative transporters are transcribed as a single mRNA. *hutF* is transcribed alone as a single gene unit. HutC functions as a transcriptional regulator of *hut* operon and an open reading frame (*hutD*) located downstream of *hutC* encodes a hypothetical protein whose function is currently unknown. The *hutC* stop codon (TGA) and *hutD* start codon (ATG) overlap, indicating that *hutC* and *hutD* are co-transcribed (Zhang and Rainey, 2007).

Comparative analysis of the *hut* genes from *Pseudomonas* strains, whose genome sequences are currently available, reveals a high degree of conservation among the *hut* catabolic genes (amino acid identity >70%), *hut* regulators (*hutCD*) and the organization of the operon (Figure 1.2). Variations are found in putative transporter genes, which are scattered in the *hutU-G* operon (Figure 1.2). There are two copies of *hutH* in the *hut* locus of *P. fluorescens* SBW25. These two copies share 36% and 87% amino acid sequence identity with characterized HutH from *P. putida* and are also present within the *hut* locus of other genome-sequenced *Pseudomonas* strains with the exception of *P. putida* KT2440 (Zhang and Rainey, 2007). However, deletion analysis of *hutH1* and *hutH2* in *P. fluorescens* SBW25 showed that only one copy (*hutH2*) encodes a functional histidase and is required for bacterial growth on histidine (Zhang and Rainey, 2007). In all the genome-sequenced *Pseudomonas*, *hutF* is located upstream of the *hutCD* operon and transcribed at the opposite orientation. Notably, transcription of *hutG* in *P. putida* ATCC12633 is also controlled by an additional weak promoter, which is induced by its own substrate formylglutamate (Hu and Phillips, 1988; Hu et al., 1989).

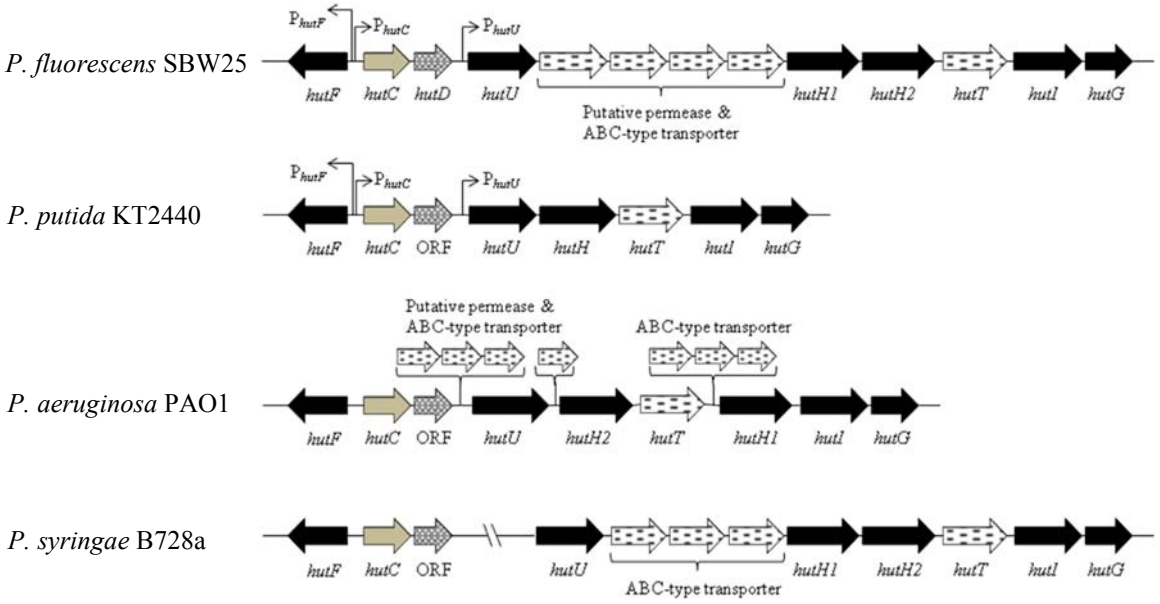

Figure 1.2. Genetic and transcriptional organization of *hut* genes in *Pseudomonas* species (Itoh et al., 2007). Metabolic *hut* genes are shown as black arrows. Regulator genes are shown as gray (*hutC*) and crosshatched (*hutD*) arrows. Stippled arrows represent putative transporters. The transcriptional orientation is indicated by arrows.

1.3 Regulation of histidine utilization (*hut*) genes

Expression of the *hut* enzymes is controlled by both specific induction (in response to the presence of histidine) and general induction (mediated by global regulators that sense the physiological status of each cell and presence of other nutrients in the medium). Specific induction of the three *hut* operons is mediated by the HutC repressor, which possesses the highly conserved helix-turn-helix DNA-binding motif (Allison and Phillips, 1990). HutC binds to the operator sites of the *hut* promoter regions to repress *hut* gene transcription in the absence of histidine. HutC binding sequences have been determined by DNase I footprint analysis in *P. putida* ATCC12633: 5'-CCATGCTTGTACATACAAGTAAAG-3'(palindromic sequences are underlined) (Allison and Phillips, 1990). Repression by HutC is relieved by urocanate, the first intermediate of the histidine degradation pathway. Therefore, histidine-induced *hut* expression requires functional histidase (HutH) activity, which converts histidine to urocanate (Zhang and Rainey, 2007).

General induction of the *hut* genes is complex and involves two two-component signal transduction systems CbrAB and NtrBC (Zhang and Rainey, 2008). When growing on histidine as the sole source of carbon or carbon and nitrogen, the *hutU-G* operon is transcribed by a sigma-54 type promoter and the transcription requires CbrAB. However, when histidine is utilized as the sole nitrogen source, either CbrAB or NtrBC system can activate the *hutU-G* operon and the transcription is controlled by a sigma-70 type promoter.

1.4 The role of HutD in histidine utilization

hutD is located downstream of *hutC* in an overlapped manner (Figure 1.2). It encodes a protein of 186 amino acids belonging to a group of uncharacterized proteins that are highly conserved in bacteria (Pfam0596). The molecular weight of HutD is estimated to be ~20.24 kDa. An alignment of HutD sequences from closely related bacteria is shown in Figure 1.3. There are 25 identical residues across eleven HutD sequences. The crystal structure of HutD (PA5104) from *P. aeruginosa* PAO1 has been determined (PDB:1y11). The asymmetric unit of the crystal contains four chains that are folded into four domains. The SCOP classification analysis shows that each chain consists of double-stranded β-helices. Although the structure of PA5104 is available it provides little information as to its function.

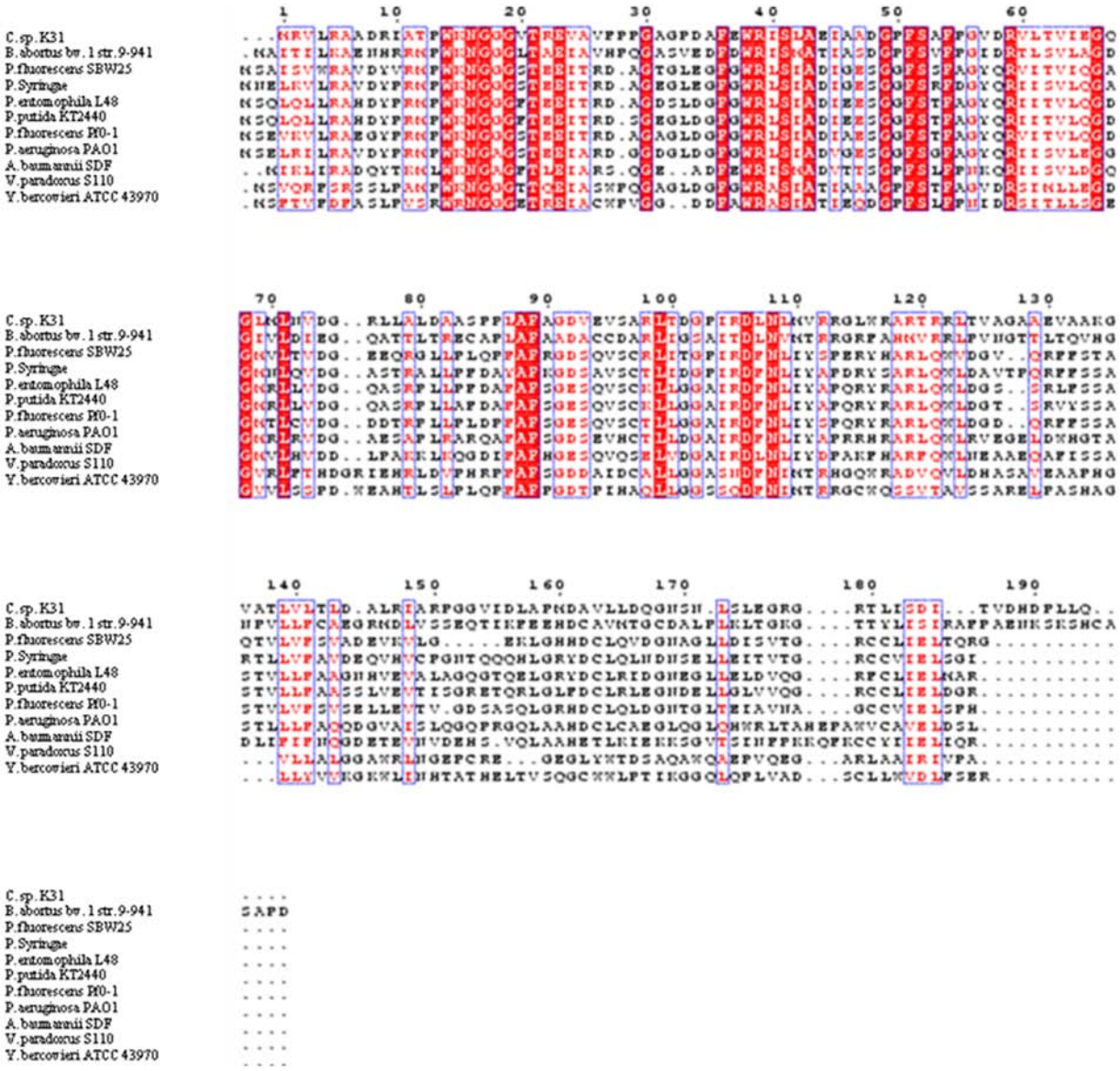

Figure 1.3. Multiple sequence alignment of HutD sequence homologues. Sequences are aligned using ClustalW2 (Larkin et al., 2007) and the figure is generated using ESPript (Gouet et al., 1999). Conserved residues are boxed and identical residues are highlighted on a red background.

Recently, the *hutD* gene in *P. fluorescens* SBW25 has been genetically characterized (Zhang and Rainey, 2007). The involvement of *hutD* in histidine (and urocanate) utilization was demonstrated by mutational analysis: the *hutD* deletion mutant grows slowly on histidine or urocanate compared with the wild-type; the *hutD* mutant is compromised in competitive growth with the wild-type in laboratory media with histidine or urocanate as the sole carbon and nitrogen source. Moreover, Zhang and Rainey (2007) showed that *hutD* functions independently of *hutC*. If HutD acts via

protein-protein interaction with HutC as predicated by their genetic organization, the double deletion mutant of *hutC* and *hutD* would display the same phenotype as Δ*hutC* mutant. In fact the Δ*hutCD* mutant expressed an intermediate phenotype compared to Δ*hutC* and Δ*hutD* indicating that HutC is not required for HutD function.

1.5 The 'governor' model of HutD action

Zhang and Rainey (2007) attempted to obtain insight into HutD function and performed a range of transcriptional and fitness assays from which they concluded that HutD functions as a governor of gene expression, preventing over-activation of *hut* expression. The most compelling evidence of this hypothesis came from the experiment in which the fitness of Δ*hutC*, Δ*hutD* and Δ*hutCD* mutants (each relative to wild type) was determined at different histidine concentrations. The fitness of Δ*hutD* and Δ*hutCD* mutants decreases with increasing concentration of histidine while the fitness of Δ*hutC* mutants increases with increasing histidine concentration (Figure 1.4). These fitness data suggest the 'governor' model of HutD action in the activation of *hut* operon. The biological need for a governor may relate to the potentially harmful effects of high rate of histidine catabolism. One of the consequences resulting from the high levels of *hut* activity is the build-up of intracellular ammonium (Zhang and Rainey, 2007).

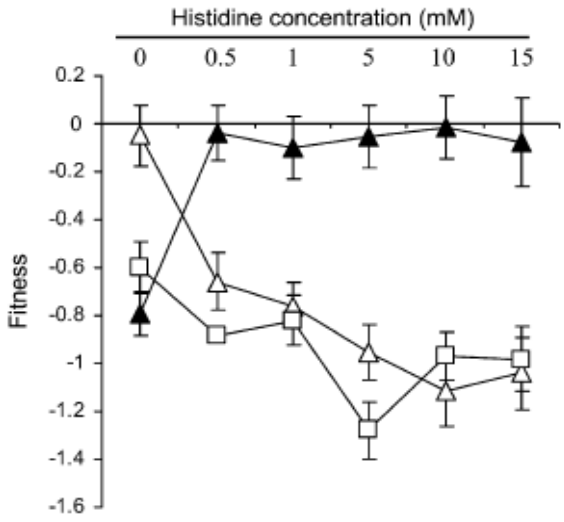

Figure 1.4. Relative fitness of Δ*hutC*, Δ*hutD* and Δ*hutCD* mutants. Fitness of Δ*hutC* (solid triangles), Δ*hutD* (open triangle) and Δ*hutCD* (open squares) mutants relative to *lacZ*-marked *P. fluorescens* SBW25 grown on M9 salts medium supplemented with 5 mM glutamate and varying concentration of histidine (Zhang and Rainey, 2007).

1.6 Deducing protein function from structural information

Structural information, which reveals the shape and surface of proteins, can sometimes provide clues as to biochemical function. Once the structure is available the challenge is to elucidate the exact biological functions of proteins *in vivo*. Structure comparison is a useful approach to this problem since there is a limited number of protein families/folds (Thornton et al., 2000). The biochemical and biological function of proteins can sometimes be inferred because of significant structural similarities. The locations of catalytic residues, ligand binding and active sites of numbers of proteins have been predicted based on structural information (Orengo et al., 1999; Thornton et al., 2000). For example, the structure of a protein (MJ0226) from *Methanococcus jannaschii* shows homology to a nucleotide binding protein. This led to the hypothesis that MJ0226 has nucleotide triphosphate activity. Such activity might protect DNA from incorporation of modified purine bases such as xanthine triphosphate and inosine triphosphate. This protein function prediction was confirmed by complementation experiments (Zhang and Kim, 2003).

1.7 Objectives of this study

The precise function of HutD remains unclear. Previous genetic data suggest that HutD is involved in the regulation of *hut* operon and a hypothesis that HutD may limit the upper level of *hut* transcription by controlling the intracellular concentration of the *hut* inducer (urocanate) has been proposed. The binding of HutD to urocanate may prevent the concentration of urocanate from exceeding a critical threshold level and the accumulation of ammonia (Zhang and Rainey, 2007). The crystal structure of HutD from *P. fluorescens* SBW25 and the structural comparison with its homologues may provide insights into the molecular mechanism of HutD action. The objectives of this study are:

1) To express and purify HutD from *P. fluorescens* SBW25
2) To crystallize HutD for structural analysis
3) To test interaction between HutD and putative ligands (histidine and urocanate)

Materials and Methods

2.1 Reagents

Reagents and chemicals were purchased from Bioline, Bio-Rad, New England Biolabs, Fermentas, GE healthcare, Sigma-Aldrich Chemicals, Invitrogen and Qiagen. All buffers and solutions were prepared using MilliQ water and filtered through a 0.45µm cellulose filter (Millipore) if required.

2.2 Bioinformatics

2.2.1 Nucleotide and protein information

The nucleotide sequence of *hutD* was obtained from *Pseudomonas fluorescens* SBW25 genome sequence (http://www.sanger.ac.uk). The protein sequence of HutD with or without an N-terminal hexa-histidine tag was analyzed for the information such as the molecular weight, extinction coefficient and theoretical isoelectric point (pI) using the online tool ProtParam available from ExPASy (Gasteiger et al., 2005) (http://www.expasy.ch/tools/protparam.html).

2.2.2 Sequence homology search and alignment

A protein sequence search for HutD was performed using NCBI BLAST (Basic Local Alignment Search Tool) server (http://blast.ncbi.nlm.nih.gov/Blast.cgi) against non-redundant protein sequences database. The program ClustalW2 was used to generate multiple sequence alignments (http://www.ebi.ac.uk/Tools/clustalw2/index.html).

2.3 Bacterial strains, plasmids and growth conditions

All strains and plasmids used in this study are listed in Table 2.1. *Pseudomonas fluorescens* and *Escherichia coli* strains were routinely grown in Luria-Bertani (LB) medium at 28ºC and 37ºC, respectively. *E. coli* transformants carrying expression plasmids pTrc99A-*hutD* were selected on LB-agar plates containing 100 µg/ml of ampicillin.

Table 2.1. Bacterial strains and plasmids used in this study

Strain or plasmid	Description	Source or reference
P. fluorescens		
SBW25	Wild-type strain	Thompson et al., (1995)
E. coli		
BL21(DE3)	F^- *ompT* *hsd*$S_B(r_B^-m_B^-)$*gal dcm* (DE3)	Invitrogen
TOP10	F^- mcrA Δ(mrr-hsdRMS-mcrBC) Φ80*lacZ* ΔM15 Δ*lac*X74 recA1 araD139 Δ(araleu) 7697 *gal*U *gal*K *rps*L (Str^R) *end*A1 *nup*G	Invitrogen
Plasmid		
pCR8/GW/TOPO	Cloning vector, Sp^R	Invitrogen
pTrc99A	Expression vector, trc promoter, Amp^R	Amann *et al*., (1988)
pTrc99A-*hutD*	pTrc99A harboring *hutD*, Amp^R	This study

2.4 DNA manipulation

2.4.1 Primer design

The nucleotide sequence of *hutD* was obtained from *Pseudomonas fluorescens* SBW25 genome sequence (http://www.sanger.ac.uk). The DNA sequence and primers were analyzed using Clone Manager Professional 5 (Sci-Ed Software) to build a restriction enzyme profile and to check for the formation of primer secondary structure and melting temperature. All primers were supplied by Invitrogen and are listed in Table 2.2.

Table 2.2. Primers used in this study

Primer	Sequence from 5' to 3'	Restriction site
HutD_TcF	ACCATGGGCCATCATCATCATCATAGT GCAATAAGCGTCTGGCG	*Nco*I
HutD_TcR	ACTGCAGCATTTTTTAACCGCGCTGGGT	*Pst*I

2.4.2 Polymerase chain reaction (PCR)

Genes of interest were amplified using the PCR from *P. fluorescens* SBW25 genomic DNA. A deoxyribonucleotide triphosphate stock was prepared from a dNTP set (Bioline) containing four separate 100 mM of dNTP solutions to generate a final concentration of 10 mM for each dNTP. The Taq DNA polymerase (Invitrogen) was used for PCR. The annealing temperatures for each pair of primers were determined based on the calculated Tm of the primers. If no PCR products or non-specific PCR products were detected at initial annealing temperatures, empirical tests were performed to find optimal annealing temperatures for the primers. The preparation of a typical 50 µl of PCR reaction was shown in Table 2.3. PCR reactions were carried out using a gradient thermal Palm-Cycler™ (Corbett Life Science) and the reaction conditions were shown in Table 2.4.

Table 2.3. Reagents for a 50 µl PCR reaction

	Volume (µl)	**Final Concentration**
10x Buffer	5	1x
$MgCl_2$ (50 mM)	1.5	1.5 mM
dNTP (10 mM)	1	0.2 mM
Forward Primer (10 pmol/µl)	1	0.2 pmol/µl
Reverse Primer (10 pmol/µl)	1	0.2 pmol/µl
Taq DNA Polymerase (5 U/µl)	0.2	1 U
Template DNA	5	--
MilliQ H_2O	35.3	--
Total Volume	50	--

Table 2.4. Typical PCR reaction conditions

	Temperature	**Time**	**Cycles**
Initial Denaturation	94ºC	3 min	1x
Denaturation	94ºC	45 s	30x
Annealing	56 ºC	45 s	
Elongation	72 ºC	1 min per kb	
Final Elongation	72 ºC	10 min	1x
Hold	4ºC		--

2.4.3 DNA transformation

To facilitate cloning of PCR products into expression vectors, the PCR products were firstly cloned into pCR®8/GW/TOPO® vectors using pCR®8/GW/TOPO® TA® Cloning Kit (Invitrogen). The desired insert DNA was then excised from the pCR®8/GW/TOPO® vectors by restriction digestion and finally ligated into the expression vectors.

2.4.4 Preparation of electrocompetent *E. coli* cells

The bacterial strain *E. coli* (BL21) from -80ºC glycerol-saline stocks was streaked out on a LB plate and grown at 37ºC overnight. A single colony from the plate was inoculated into 10 ml of LB and grown at 37ºC with shaking at 180 rpm overnight. 5 ml of overnight culture was inoculated into 500 ml of LB and grown at 37ºC with shaking at 120 rpm to an OD_{600} of 0.6-0.7. Cells were chilled on ice for 20 minutes and harvested at 4,000 g for 20 minutes at 4ºC. The supernatant was discarded and the cell pellet was resuspended in 250 ml of chilled 10% glycerol. The cells were centrifuged at 4,000 g for 20 minutes at 4ºC and supernatant was discarded. The cell pellet was further washed with 125 ml of chilled 10% glycerol twice. The cells were centrifuged at 4,000 g for 20 minutes at 4ºC and the supernatant was discarded. The cell pellet was resuspended in 2 ml of chilled 10% glycerol. 50 µl of aliquots were made and stored at -80ºC.

2.4.5 Glycerol-saline stock

Glycerol-saline stock was made for long-term storage of bacteria. The bacteria were inoculated in LB containing the appropriate antibiotic and grown at 37ºC with shaking. 1 ml of bacterial culture was added to 800 µl of glycerol saline, mixed thoroughly and stored at -80ºC.

Glycerol-saline

0.85% (w/v)	NaCl
70% (v/v)	Glycerol

2.4.6 Electroporation

2 µl of plasmid DNA or ligation products was added to 50 µl of electrocompetent cells that had been thawed on ice. The cells were placed between 0.1 cm electrodes of a pre-chilled gapped Gene Pulser® cuvette (Bio-Rad) and electroporated using Electroporator 2510 (Eppendorf) at 1.8 kV. 800 µl of SOC medium was immediately added and the electroporated cells were transferred to a 1.5 ml sterile eppendorf tube. The cells were incubated at 37ºC with shaking at 180 rpm for 1 hour. The culture was spread onto LB plates containing the appropriate antibiotic and incubated at 37ºC overnight. After incubation, colonies of transformants were inoculated into 5 ml of LB containing the appropriate antibiotic and grown 37ºC with shaking at 180 rpm overnight. Plasmid DNA was isolated from these cultures.

S.O.C medium

2% Bacto Tryptone	10 mM $MgCl_2$
0.5% Yeast Extract	10 mM $MgSO_4$
20 mM Glucose	10 mM NaCl
	2.5 mM KCl

2.4.7 Preparation of plasmid DNA

Plasmid DNA was extracted from overnight bacterial cultures using QIAprep Spin Miniprep Kit (Qiagen) according to the manufacturer's instructions. 30µl or 50µl of MilliQ H_2O was used to elute DNA.

2.4.8 Restriction enzyme digestion

DNA was digested with restriction enzymes (Invitrogen) in the appropriate REact buffers at 37ºC for at least 2 hours or overnight.

2.4.9 Agarose gel electrophoresis

DNA fragments were separated on 1% agarose gels in 1x TAE buffer (UltraPure™, Invitrogen) containing 1x SYBR Safe™ DNA gel stain (Invitrogen). Samples were mixed with 6x DNA loading dye (Fermentas) at the ratio of 1:5 prior to loading onto the gel. Gels were run at 140 volts for 30-60 minutes. Lambda DNA/EcoRI+HindIII marker (Fermentas) was also loaded to estimate the size of DNA fragments.

Visualization of DNA was undertaken using UV light generated from a High Performance Transilluminators (UVP, LLC) and gels were photographed using DigiDoc-It™ Imaging System with Doc-It LS Analysis Software (UVP, LLC).

2.4.10 DNA purification

DNA samples were subjected to the agarose gel electrophoresis. The desired band was excised from the gel and purified using QIAquick Gel Extraction kit (Qiagen).

2.4.11 DNA ligation

Ligation of DNA inserts with plasmid vectors at the molar ratio of 3:1 was performed using T4 DNA ligase (Invitrogen). Reactions were incubated at 16ºC overnight.

2.5 Protein expression and solubility tests

2.5.1 Small-scale protein expression

A single colony from an LB plate with the appropriate antibiotic was inoculated into 5 ml of LB containing the appropriate antibiotic, and grown at 37ºC with shaking at 180 rpm overnight. 1 ml of overnight bacterial culture was inoculated into 50 ml of LB containing the appropriate antibiotic in a 250 ml flask. The bacterial culture was grown at 37ºC with shaking at 180 rpm to an optical density (OD_{600}) of 0.6-0.7 and then the culture was split equally into two parts. IPTG (isopropyl-β-D-thiogalactopyranoside) was added to a final concentration of 1mM to one of the cultures. The bacterial cultures (one induced, one uninduced) were incubated at 37ºC or 25ºC for the protein induction. 1 ml of aliquot was taken from each culture before induction and at 1 hour, 2 hours, 4 hours and overnight after induction. Samples of aliquots were centrifuged at 13,000 rpm for 2 minutes and the bacterial culture was harvested at 4,000 g for 20 minutes. The supernatant was discarded and cell pellets were stored at -20ºC until use.

2.5.2 Large-scale protein expression

A single colony from an LB plate with the appropriate antibiotic was inoculated into 10 ml of LB containing the appropriate antibiotic, and grown at 37ºC with shaking at

180 rpm overnight. 10 ml of overnight bacterial culture was inoculated into 500 ml of LB containing the appropriate antibiotic in a 2 L flask. The bacterial culture was grown at 37ºC with shaking at 140 rpm to an OD_{600} of 0.6-0.7 and IPTG was added to a final concentration of 1mM. The bacterial culture was incubated at 25ºC overnight for the protein induction and was harvested at 4,000 g for 20 minutes. The supernatant was discarded and cell pellets were stored at -20ºC until use.

2.5.3 Cell lysis and protein solubility tests

Frozen cell pellets were thawed on ice and resuspended in 10 ml of lysis buffer. They were incubated on ice for 30 minutes when lysozyme (1.0 mg/ml), DNase I (20µg/ml) and PMSF (0.1 mM) were added. Cells were lysed by sonication on ice at 5x 60s bursts with 60s pauses using the Microtip™ of Sonicator S-4000 Ultrasonic Liquid Processor (Misonix, Inc) at amplitude of 60 mV. The resulting cell lysate was centrifuged at 4,000 g for 20 minutes. The supernatant was collected and retained as the soluble fraction for purification by nickel-nitrilotriacetic acid (Ni-NTA) metal affinity chromatography while the pellet was resuspended in 10 ml of lysis buffer and retained as the insoluble fraction. The soluble and insoluble samples were mixed with 2x sample buffer at 1:1 ratio and were subjected to SDS-PAGE.

Lysis buffer

20 mM	Imidazole
500 mM	NaCl
20 mM	HEPES, pH 7.5

2.6 Sodium dodecyl Sulfate – polyacrylamide gel Electrophoresis

2.6.1 Gel preparation

Protein samples were analyzed by SDS-PAGE (Lammili, 1970) using the XCell *SureLock*™ mini-cell system (Invitrogen). The components of buffers, 5% stacking gels and 12% or 16% resolving gels are listed below.

10x SDS-PAGE running buffer, pH8.3

30.3 g	Tris base
144.0 g	Glycine
10.0 g	Sodium dodecyl sulfate (SDS)
Added MilliQ H_2O up to 1L	

2x Sample buffer (Reducing buffer)

125 mM	Tris-HCl, pH6.8
20%	Glycerol
4% (w/v)	SDS
10% (v/v)	β-mercaptoethanol
0.02 (w/v)	Bromophenol blue

Stacking gel (5% acrylamide)

5.7 ml	MilliQ H_2O
1.7 ml	30% Acrylamide (29:1 acrylamide:bis)
2.5 ml	0.5 M Tris-HCl, pH6.8
0.1 ml	10% (w/v) SDS
50 µl	10% (w/v) Ammonium persulfate (APS)
10 µl	TEMED

Resolving gel (12% acrylamide)

3.4 ml	MilliQ H_2O
4.0 ml	30% Acrylamide (29:1 acrylamide:bis)
2.5 ml	0.5 M Tris-HCl, pH6.8
0.1 ml	10% (w/v) SDS
50 µl	10% (w/v) APS
5 µl	TEMED

Resolving gel (16% acrylamide)

2.1 ml	MilliQ H_2O
5.3 ml	30% Acrylamide (29:1 acrylamide:bis)
2.5 ml	0.5 M Tris-HCl, pH6.8
0.1 ml	10% (w/v) SDS
50 µl	10% (w/v) APS
5 µl	TEMED

2.6.2 Sample preparation, gel running and staining

The pellet of whole cells was resuspended in 100 µl of 2x sample buffer. The purified protein sample was mixed with 2x sample buffer at 1:1 ratio. Samples were heated to 95ºC for 5 minutes prior to being loaded onto a stacking gel. SDS-PAGE was run at 150V until the front dye reached the bottom of a resolving gel. Gels were stained with Coomassie brilliant blue for 1 hour and destained overnight, shaken gently at room temperature.

Coomassie blue stain

0.125%	Coomassie brilliant blue R250
50%	Methanol
10%	Acetic acid

Filtered the mixture

Detain

30%	Methanol
10%	Acetic acid

2.7 purification of hexa-histidine-tagged HutD

Hexa-histidine-tagged (His_6-tagged) HutD was purified by Ni-NTA affinity chromatography. A 1 ml of HisTrap™ HP (GE Healthcare) affinity column was firstly washed with 5 ml of MilliQ H_2O and equilibrated with 5 ml of binding buffer using a syringe. The soluble fraction of cell lysate was loaded onto the column. The column was then washed with 10 ml of binding buffer and eluted with a stepped gradient of elution buffer, firstly with 75 mM imidazole, then 300 mM imidazole and finally 500 mM imidazole. The purification was conducted at a flow rate of 1 ml/min.

Binding buffer

20 mM Imidazole
500 mM NaCl
20 mM HEPES, pH 7.5

Elution buffer 1

75 mM Imidazole
500 mM NaCl
20 mM HEPES, pH 7.5

Elution buffer 2

300 mM Imidazole
500 mM NaCl
20 mM HEPES, pH 7.5

Elution buffer 3

500 mM Imidazole
500 mM NaCl
20 mM HEPES, pH 7.5

2.8 Concentration of proteins and buffer exchange

The protein HutD was concentrated using Vivaspin 6 concentrators (GE healthcare) with 10 kDa molecular weight cut off. The protein was loaded into the concentrator and centrifuged at 4,000 g at 4ºC until the desired concentration of protein was reached. For the buffer exchange, the protein was repeatedly diluted with the new buffer in the Vivaspin concentrator until the components of old buffer became negligible. The concentrated HutD in the storage buffer was stored at -80ºC.

Storage buffer

20 mM Sodium phosphate, pH 7.5
500 mM NaCl

2.9 Size-exclusion chromatography

The molecular weight of HutD was accurately estimated by size exclusion chromatography. The size exclusion chromatography was carried out using a Superdex™ 75 10/300 GL column (GE Healthcare). Three molecular standards, ribonuclease A, ovalbumin and conalbumin, from Gel Filtration Calibration Kit LMW

(Low Molecular Weight) (GE Healthcare) were prepared in the buffer (20 mM HEPES pH7.5 and 150 mM NaCl) at a final concentration of 3 mg/ml, 4 mg/ml and 3 mg/ml, respectively. 200 µl of molecular standard mixture was used to calibrate the gel filtration column. The column has a geometric volume of 24 ml and the void volume (equals to elution volume) of the column was determined by loading 200 µl of Blue Dextran 2000 (1 mg/ml) into the column. The size exclusion chromatography was performed using an ÄKTA Prime™ system (GE Healthcare) with a flow rate of 1 ml/min. The standard curve was prepared by plotting K_{av} versus logMW, where K_{av} = (Ve-Vo)/(Vc-Vo), Ve = elution volume, Vo = column void volume and Vc = geometric column volume. This standard curve was used to estimate the molecular weight of protein.

2.10 Determination of protein concentration

2.10.1 Determination of protein concentration by Bradford assay

The protein concentration was estimated by Bradford assay (Bradford, 1976). A series of BSA protein standards (0 – 2 mg/ml) was prepared in the buffer (20 mM HEPES pH7.5 and 150 mM NaCl) used for the storage of protein and 10-fold dilution of samples containing protein of unknown concentration was made in the same buffer. 1 ml of Quick Start™ Bradford Dye Reagent (1x) (Bio-Rad) was added to 20 µl of BSA protein standards and protein samples and incubated at room temperature for 15 minutes. The absorbance of each sample was measured at 595 nm using a spectrophotometer and a standard curve was made by plotting absorbance versus BSA standards. The concentration of protein was estimated using this standard curve.

2.10.2 Determination of protein concentration by Beer-Lambert equation

The protein concentration was determined using a Nanodrop ND-1000 Spectrophotometer (Nanodrop™). The UV absorbance of the protein at 280 nm was measured. The protein concentration was calculated based on the Beer-Lambert equation

$$A = \varepsilon \cdot c \cdot l$$

where A is the absorbance at 280 nm, ε is the molar extinction coefficient (L mol^{-1} cm^{-1}), c is the protein concentration (mol L^{-1}) and l is the path length (cm). The molar

extinction coefficient of protein was calculated using the online tool ProtParam (Gasteiger et al., 2005).

2.11 Protein function tests

2.11.1 Thermal shift assay

The interaction between ligands and HutD was monitored by thermal shift assay based on the differential scanning fluorimetry (Niesen, et al., 2007). 100 μg/ml of HutD in the buffer containing 20 mM HEPES pH7.5 and 150 mM NaCl, SYPRO orange and the appropriate concentration of ligands were mixed in total volume of 20 μl and the solution was added to the wells of a IQ 96-well PCR plate (Bio-Rad). The thermal shift assay was conducted in the MyiQ real-time PCR Detection System (Bio-Rad) with an excitation wavelength of 490 nm and an emission wavelength of 530 nm. The sample in the PCR plate was heated from 25 to 95ºC with a heating rate of 1 ºC/min.

2.11.2 Isothermal titration calorimetry

Isothermal titration calorimetry (ITC) was performed to directly study the thermodynamics of biological molecules interactions. The interaction between biological molecules is often accompanied by either heat absorption (an endothermic process) or heat release (an exothermic process). The change in heat can be measured and is often characterized as the change in the Gibbs free energy (ΔG). The ΔG associated with binding is related to the equilibrium association constant (K_A):

$$\Delta G = -RT\ln K_A = \Delta H - T\Delta S$$

Where R is the gas constant, T is the temperature in Kelvin, ΔH is the enthalpy change and ΔS is the entropy change. The ΔG, ΔH, ΔS and K_A values can be measured by ITC (Freyer and Lewis, 2008). The ITC measurement was carried out at 20ºC using a VP-ITC MicroCalorimeter (MicroCal). HutD (50 μM) was dialysed in 4 L of the protein storage buffer (20 mM HEPES pH7.5 and 150 mM NaCl) overnight. The putative ligands (100 mM) were dissolved and dialysed in the same buffer used

for protein dialysis overnight. The concentration of the protein and ligands was measured after dialysis. All solutions were degassed before the titration.

The protein (~1.4 ml) was loaded into a sample cell while the ligand (~300 µl) was loaded into an injector. 2 µl of preliminary injection was performed prior to 28 injections of 10 µl into the sample cell with 5 minutes intervals. The reference power was 20 µcal/sec by default. The change in heat was measured for each injection. A control experiment was carried out by injecting the ligand into buffer only. The ITC data were analysed using MicroCal Origin 7 (Origin®).

2.12 Protein crystallization

2.12.1 Initial crystallization trials

The initial crystallization trial of proteins was performed using a flexible medium-throughput approach (Moreland et al., 2005). His_6-HutD purified from Ni-NTA chromatography was centrifuged at 17,000 g for 5 minutes at 4ºC prior to being dispensed. The in-house screens containing a total of 480 conditions were set up in five 96-well Intelli-Plates (Hampton Research) for initial screening of a target protein. The crystallization precipitant solutions were assembled and dispensed (50 µl of each solution) into the reservoir wells of Interlli-Plates by a MultiPROBE II HT/EX liquid-handling robot (Perkin-Elmer). The Interlli-Plates were then transferred to a Cartesian nanolitre-dispensing robot (Cartesian™ Dispensing Systems), which dispensed 100 nl drops of the protein and well solution into the crystallization wells. The five 96-well Intelli-Plates were sealed with Clearseal film (Hampton Research). The sitting-drop vapour-diffusion crystallization was carried out at 18ºC and relative humidity to minimize evaporation. The drops were immediately examined under a microscope after being set down and the crystallization process was then periodically observed and scored: 0- clear drop; 1- glass, dust or fibre; 2- brown precipitate/denatured protein; 3- heavy amorphous precipitate; 4- light amorphous precipitate; 5- non-amorphous precipitate; 6- gelatinous precipitate; 7- phase separation/oil; 8- spherulites; 9- micro-crystals; 10- needles; 11- plates; 12- crystals.

2.12.2 Optimization of crystallization conditions

When successful crystallization conditions were found in the initial crystallization trials, fine screening was performed to optimize the conditions. Fine screening was undertaken using the sitting-drop vapour-diffusion system. The concentration of promising crystallization precipitant was varied and 500 µl of the precipitant solution was pipetted into wells of a Crystalquick 24-well plate (Greiner Bio-One) and micro-bridges were placed in each well. 1 µl each of protein and precipitant solution was mixed in the micro-bridge wells and the plate was sealed with Clearseal film (Hampton Research). The crystallization process was then periodically examined to obtain larger crystals.

2.13 Protein diffraction data collection

2.13.1 Cryoprotectant test

To reduce radiation damage to protein crystals during X-ray exposure, the cryo-technique was undertaken for diffraction data collection. Cryo-solutions which consist of crystal mother liquor and a cryoprotectant such as glycerol in varying percentage (v/v) were firstly prepared. A drop of cryo-solution was collected in a nylon cryo-loop (Hampton Research) and immediately immersed in liquid nitrogen. The flash-cooled cryo-solution was subjected to X-ray radiation for 5 minutes and the resulting image was analyzed for the presence of ice rings (crystalline ice) at 2.95Å. The lowest concentration of the cryoprotectant which did not give ice rings was then used to cryoprotect protein crystals.

2.13.2 Flash freezing crystals

Protein crystals were mounted onto a nylon cryo-loop fixed (Hampton Research). To minimize the osmotic shock to them, the crystals were sequentially soaked in 2 µl of increasing concentrations of cryo-solutions for 30 s to 5 min. After soaking, the crystals were immediately transferred to a pre-cooled cryo-cane in a Dewar and flash-cooled by immersion in liquid nitrogen.

2.13.3 X-ray diffraction data collection

Home source X-ray data were collected using CuKα radiation (λ = 1.5418 Å) generated by a MicroMax™-007HF X-ray generator (Rigaku), operating at 50 kV and 100 mA equipped with Osmic VariMax-HF optics and a rotating copper anode. Protein crystals in the cryo-loop were mounted on the goniometer using a MAR345dtb mounting robotic system (MAR Research GmbH). The crystals were subjected to a stream of cold nitrogen gas at 100K – 113K with the temperature controlled by a Cobra cryosystem (Oxford Cryosystems). The diffraction data were collected by a MAR345 image plate detector (MAR Research GmbH).

2.14 Diffraction data processing

2.14.1 Indexing, integration and scaling of diffraction data

The HKL-2000 program suite consisting of *XdisplayF*, *Denzo* and *Scalepack* was performed to index, integrate and scale the diffraction data (Otwinowski and Minor, 1997). *XdisplayF* was used to visualize diffraction images and find spots. *Denzo* was used to estimate the crystal unit cell parameters, lattice type and the orientation of the crystal. These parameters were used to deduce the lattice and space group. The lattice parameters were then refined and at this point the diffraction image was examined to make sure the predicted reflections matched observed spots. During the refinement the mosaicity was determined by checking that the mosaicity histogram had correct shape and the predicted reflections were lined up with observed ones. These refined parameters from the first frame were then used to integrate the set of frames in whole dataset. Once the data had been processed with *Denzo*, *Scalepack* was performed to find the relative scale factors between images and precisely refine the crystal parameters using the whole data set. The statistical data R_{merge}, χ^2, I/σI and the data completeness were examined and if necessary, the error estimates, rejection probability error scale factor or resolution limits were altered so that the error model could fit the actual errors.

2.14.2 Unit cell content analysis

The programme Matthews_Coef which calculates the Matthews coefficient (V_M) in the CCP4 (Bailey, 1994) was performed to estimate the number of molecules in the

unit cell and solvent content (Matthews, 1968). V_M is defined as the crystal volume per unit of protein molecular weight and shows a straightforward relationship to the fractional volume of solvent in the crystal. The solvent content of crystals ranged from about 27% to 65%, with the most common value being near 43% (Matthews, 1968).

2.14.3 Phase determination using molecular replacement

Structure solution by molecular replacement (MR) was undertaken using Phaser (McCoy et al., 2007) via the CCP4 interface (Bailey, 1994). The programme Chainsaw was used to prepare the search model for the molecular replacement (Stein, 2008). The sequences of the target and search model were aligned and non-conserved residues were truncated to the gamma carbon atom in the Chainsaw. The MR solutions were judged based on the Z-score of rotation and translation function and log-likelihood gain and refined by the programme Refmac (Murshudov et al., 1997).

2.14.4 Model building and refinement

The electron density map was used in Coot for model building (Emsley and Cowtan, 2004).The model was built into 2|Fo|-|Fc| density map contoured at 1-1.5 σ and |Fo|-|Fc| difference map contoured at 2.5-3.5 σ. The built-in tools in Coot were used to visualize and adjust the model. The modified model containing altered residues, water and other solvent molecules was subsequently refined in Refmac (Murshudov et al., 1997). The values of R and R_{free} were examined to evaluate the quality of refinement. The final model was validated by Molprobity (http://molprobity.biochem.duke.edu/) (Davis et al., 2007).

2.15 Structural analysis

The protein structure was classified using SCOP (Structural Classification of Proteins) (http://scop.mrc-lmb.cam.ac.uk/scop/) (Murzin et al., 1995). The protein structure comparison was performed using Dali (http://ekhidna.biocenter.helsinki.fi/dali server/) (Holm et al., 2008) and ConSurf servers (http://consurf.tau.ac.il/) (Landau et al., 2005). The protein interface was analyzed using PISA (Protein Interfaces, Surfaces and Assemblies) (http://www.ebi.ac.uk/msd-srv/prot_int/pistart.html) (Krissinel and Henrick, 2007).

Results

3.1 Cloning of *hutD* to the expression vector pTrc99A

Plasmid pTrc99A is a general cloning vector that has been widely used for the regulated expression of genes in *E. coli* (Amann et al., 1988). As shown in Figure 3.1, it has a strong hybrid *trp*/*lac* (*tac*) promoter which activity is repressed by the $LacI^q$ repressor. Expression of the cloned gene is induced by addition of IPTG in the growth medium. Located 8 bp downstream of the *lacZ* ribosomal binding site (RBS) is a unique *Nco*I restriction site (CCATGG), which provides an ATG start codon for gene translation. It contains the multiple cloning site from pUC18 and the *rrnB* transcriptional terminator.

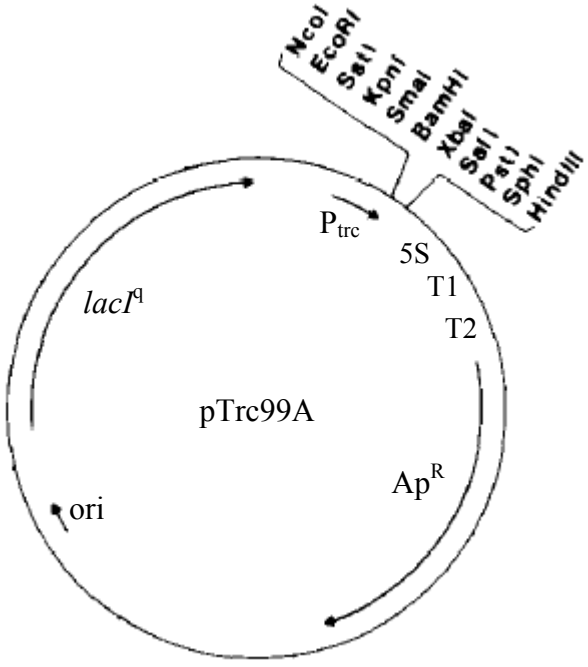

Figure 3.1. The map of pTrc99a expression vector (Amann et al., 1988). ori: origin of replication. $lacI^q$: autorepressor. P_{trc}: trc promoter. 5S: 5S rRNA. T1&T2: transcriptional terminator of the *rrnB* operon. Ap^R: ampicillin resistance gene. Direction of transcription and orientation of genes are indicated by arrows.

To express the *hutD* in pTrc99A, a pair of primers HutD_TcF (5' – ACCATGGGC**CATCATCATCATCATCAT**AGTGCAATAAGCGTCTGGCG – 3') and HutD_TcR (5' – ACTGCAGCATTTTTTAACCGCGCTGGGT – 3') were designed to amplify the coding region of the *hutD* gene from *P. fluorescens* SBW25. Restriction sites *Nco*I and *Pst*I (underlined) were incorporated into the primers to facilitate directional cloning. An N-terminal hexa-histidine tag (shown in bold letter) was introduced for subsequent purification of the HutD protein.

A ~580 bp DNA fragment was amplified by PCR using primers HutD_TcF and HutD_TcR from the genomic DNA of *P. fluorescens* SBW25 (details see Section 2.4.2). The PCR product was gel-purified and cloned into pCR®8/GW/TOPO® vectors (Invitrogen) following the manufacturer's instruction. After the sequence identity was determined by DNA sequencing using universal primers (M13 forward and T7), the *hutD* fragment was retrieved by *Nco*I/*Pst*I digestion and cloned into pTrc99A (Figure 3.2), which was also treated by *Nco*I/*Pst*I. The resulting plasmid was designated pTrc99A-*hutD*. Restriction analysis of pTrc99A-*hutD* (digested by *Nco*I/*Pst*I) produced two bands: a 2.8 kb band for the vector pTrc99A and a 580 bp fragment insert for *hutD* (Figure 3.3).

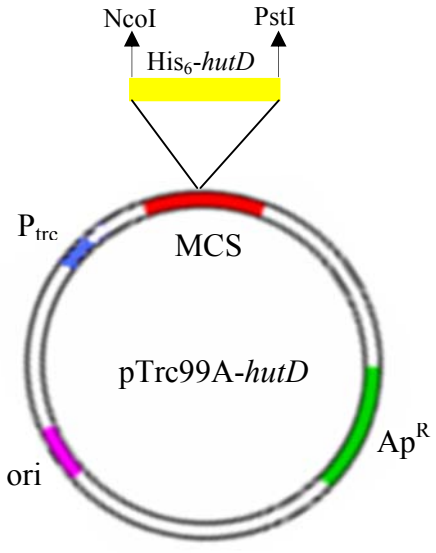

Figure 3.2. Construction of HutD expression plasmid pTrc99A-*hutD*. PCR products of N-terminal hexa-histidine tagged *hutD* (His_6-*hutD*) and expression vectors pTrc99A were digested with *Nco*I and *Pst*I, and then ligated to generate pTrc99A-*hutD* for HutD overexpression. MSC: multiple cloning site. P_{trc}: *trc* promoter. Ap^R: ampicillin resistance gene.

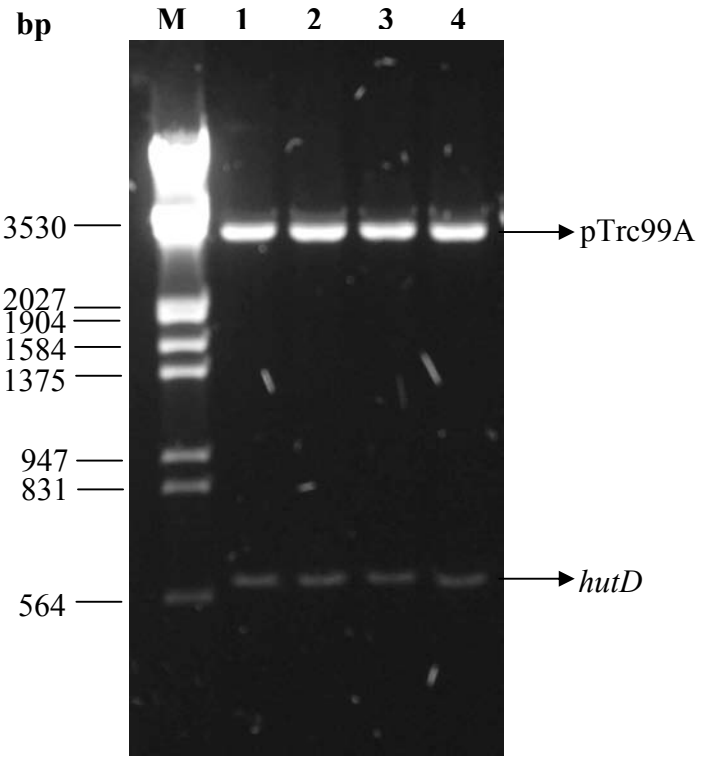

Figure 3.3. Restriction digestion of pTrc99A-*hutD*. Expression plasmid pTrc99A-*hutD* was digested with *Nco*I and *Pst*I. Lane 1-4: pTrc99A-*hutD* cut with both *Nco*I and *Pst*I. M: DNA ladder.

3.2 Protein expression and purification

3.2.1 Small-scale expression and solubility of HutD

To express *hutD* in *E. coli*, the recombinant plasmid pTrc99A-*hutD* was transformed into *E. coli* BL21 (DE3), a general host for overexpression of foreign proteins. An initial assay was then performed by growing the bacteria in 50 ml LB broth to OD_{600} of 0.6 – 0.7 and inducing the expression of *hutD* with 1.0 mM IPTG at 37ºC. After the IPTG induction, aliquots were taken at different time and subjected to SDS-PAGE analysis. Results are shown in Figure 3.4. A band at the molecular weight of ~20 kDa

was found in all samples but the intensity was much higher in the induced cells compared to the controls (uninduced cells and induced cells without pTrc99A-*hutD*). The predicted molecular weight of His_6-HutD is 21.2 kDa. The data thus suggest that *hutD* is successfully overexpressed at 37ºC.

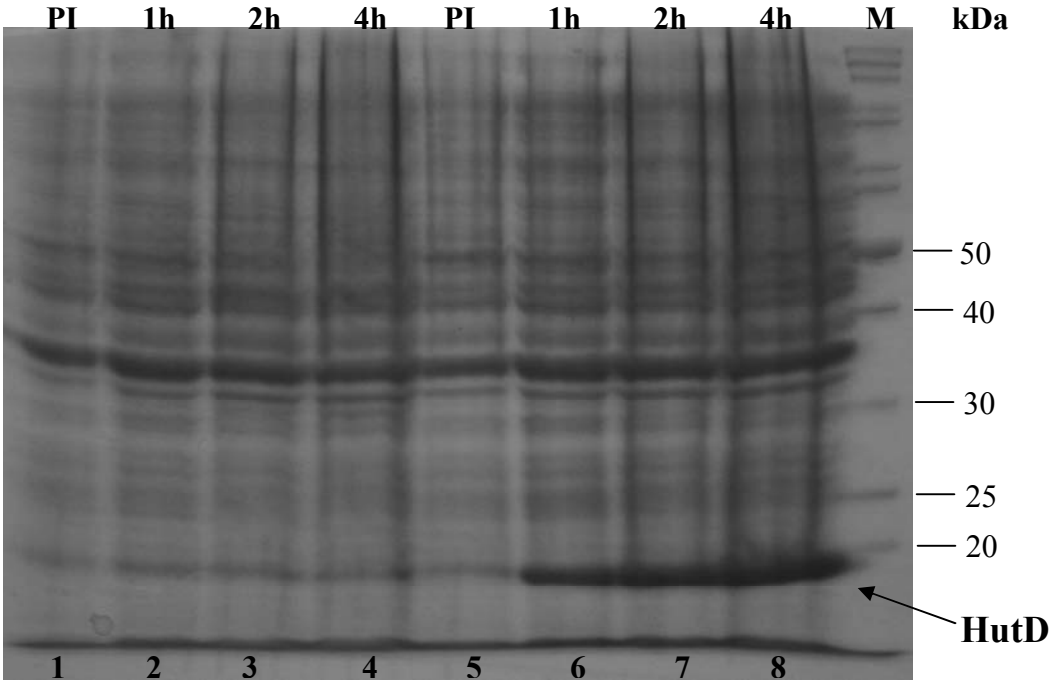

Figure 3.4. SDS-PAGE analysis of HutD expression at 37ºC. Aliquots of bacterial culture were taken before IPTG induction and after induction at 1 hour, 2 hours and 4 hours. Proteins were separated by 12% SDS-PAGE and visualised by staining with Coomassie blue. Lane 1-4: cells not harbouring HutD expression plasmids. Lane 5-8: cells containing HutD expression plasmids. PI: pre-induction; M: protein molecular marker.

Next the solubility of the overexpressed HutD was tested. IPTG-induced cells were treated with lysozyme and sonication (details see Section 2.5.3). The soluble and insoluble fractions were then analysed by SDS-PAGE. Results shown in Figure 3.5 indicated that only a small proportion of HutD was soluble.

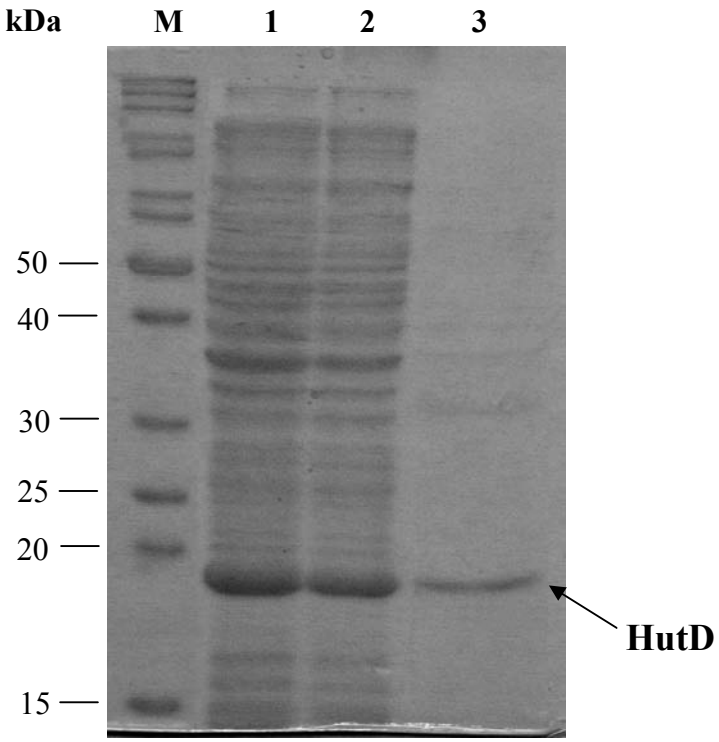

Figure 3.5. SDS-PAGE analysis of the solubility of HutD expressed at 37ºC. Bacterial cells were induced with 1.0 mM IPTG at 37ºC. The induced whole cells were lysed. The insoluble and soluble fractions were separated by centrifugation and analysed by 12% SDS-PAGE. M: protein molecular weight marker. Lane 1: induced whole cell lysate. Lane 2: insoluble fraction of cell lysate. Lane 3: soluble fraction of cell lysate.

Usually protein solubility can be increased by growing cells at low temperatures (Donovan et al., 1996). The expression and solubility of HutD were tested using the similar protocols except that the bacteria were grown at 25ºC instead of 37ºC. As expected, HutD was successfully overexpressed (Figure 3.6) and most of HutD was soluble (Figure 3.7). Thus, reducing the growth temperature from 37ºC to 25ºC significantly improved the solubility of HutD.

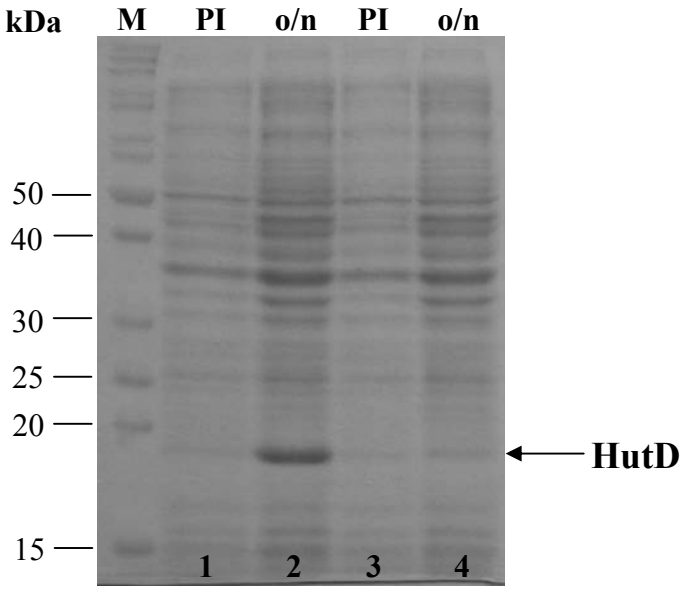

Figure 3.6. SDS-PAGE analysis of HutD expression at 25ºC. Aliquots of bacterial culture were taken before IPTG induction and after induction overnight. Proteins were separated by 12% SDS-PAGE and visualised by staining with Coomassie blue. M: protein molecular marker. PI: pre-induction. Lane 1-2: cells harbouring HutD expression plasmids. Lane 3-4: cells not containing HutD expression plasmids.

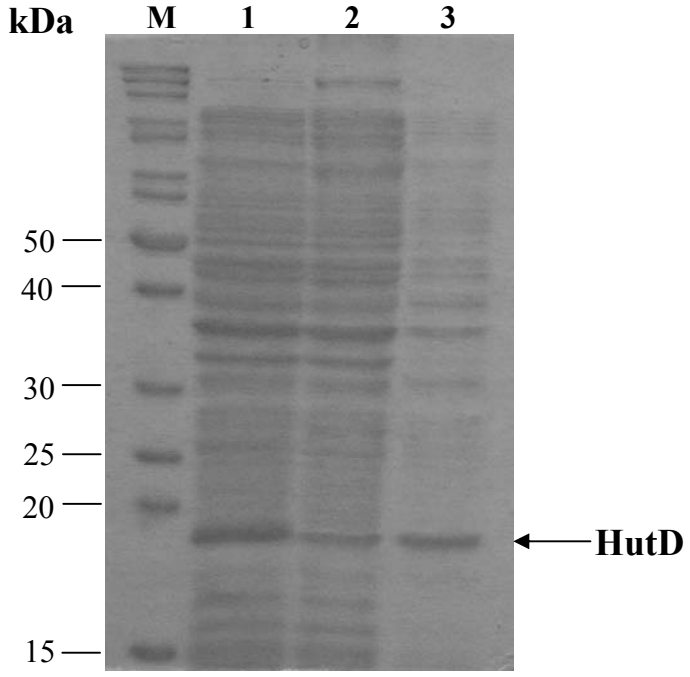

Figure 3.7. SDS-PAGE analysis of the solubility of HutD expressed at 25ºC. Bacterial cells were induced with 1.0 mM IPTG at 25ºC. The induced whole cells were lysed. The insoluble and soluble fractions were separated by centrifugation and analysed by 12% SDS-PAGE. Lane 1: induced whole cell lysate. Lane 2: insoluble fraction of cell lysate. Lane 3: soluble fraction of cell lysate. M: protein molecular weight marker.

3.2.2 Large-scale expression and purification of HutD

As the solubility of HutD increased when expressed at 25ºC in the initial test, the large-scale expression of HutD was carried out at this temperature (details see Section 2.5.2). *E. coli* BL21 (DE3) containing pTrc99A-*hutD* was grown in 500 ml LB broth in a two-litre flask. Bacteria were cultivated at 25ºC with shaking at 140 rpm. After overnight IPTG (1.0 mM) induction cells were harvested and lysed by using lysozyme and sonication. The soluble and insoluble fractions of cell lysate were separated by centrifugation.

The His_6-tagged HutD protein was subsequently purified from the soluble fraction of cell lysate by Ni-NTA affinity chromatography (details see Section 2.7). The soluble fraction of the cell lysate was loaded onto a Ni-NTA affinity column in the presence of 20 mM imidazole. The column was washed with the binding buffer containing 20 mM imidazole and then a stepped imidazole gradient (75 mM, 300 mM and 500 mM) was used to remove contaminants and elute HutD from the column. The eluted fractions were collected and analysed by SDS-PAGE. As shown in Figure 3.8, HutD was successfully purified from most other contaminating proteins.

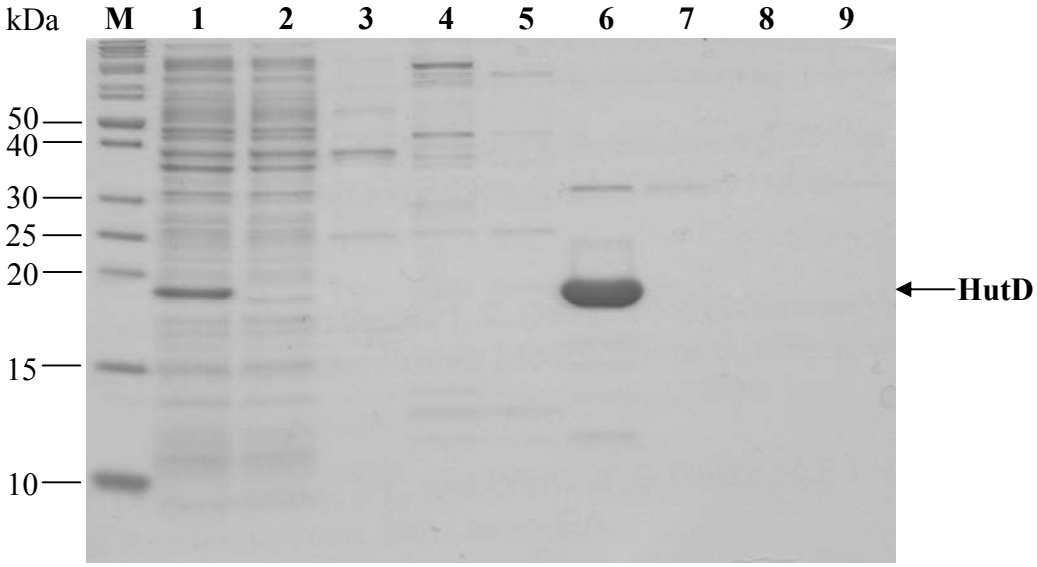

Figure 3.8. Purification of His6-HutD by Ni-NTA affinity chromatography. The soluble fraction of cell lysate was loaded to an affinity column and eluted with elution buffer containing a stepped imidazole gradient. The eluted fractions were analysed by SDS-PAGE. M: protein molecular weight marker. Lane 1: soluble fraction of cell lysate. Lane 2: fraction washed with 20 mM imidazole. Lane 3-4: fractions eluted with 75 mM imidazole. Lane 5-7: fractions eluted with 300 mM imidazole. Lane 8-9: fractions eluted with 500 mM imidazole.

3.3 Analytical size-exclusion chromatography

The molecular weight and multimerization state of His_6-HutD was determined by size-exclusion chromatography using a S75 10/300 GL column (details see Section 2.9). The column was firstly calibrated with molecular standards: ribonuclease A (13.7 kDa), ovalbumin (43.0 kDa) and conalbumin (75.0 kDa). The void volume (Vo) of the column is 9.637 ml and the elution volumes (Ve) of ribonuclease A, ovalbumin and conalbumin are 16.516 ml, 12.705 ml and 11.759 ml respectively (Figure 3.9A). According to the equation K_{av} = (Ve-Vo)/(Vc-Vo), a standard curve of K_{av} versus logMW was plotted (Figure 3.9B). The purified His_6-HutD was loaded onto the column and only one peak was observed (Ve = 12.911 ml) (Figure 3.9C). Based on the standard curve and the elution volume of HutD, the molecular weight of His_6-HutD was determined as 45.8 kDa which is almost two times larger than the predicted size (21.2 kDa). From these experiments, we can conclude that HutD forms a dimer in the solution.

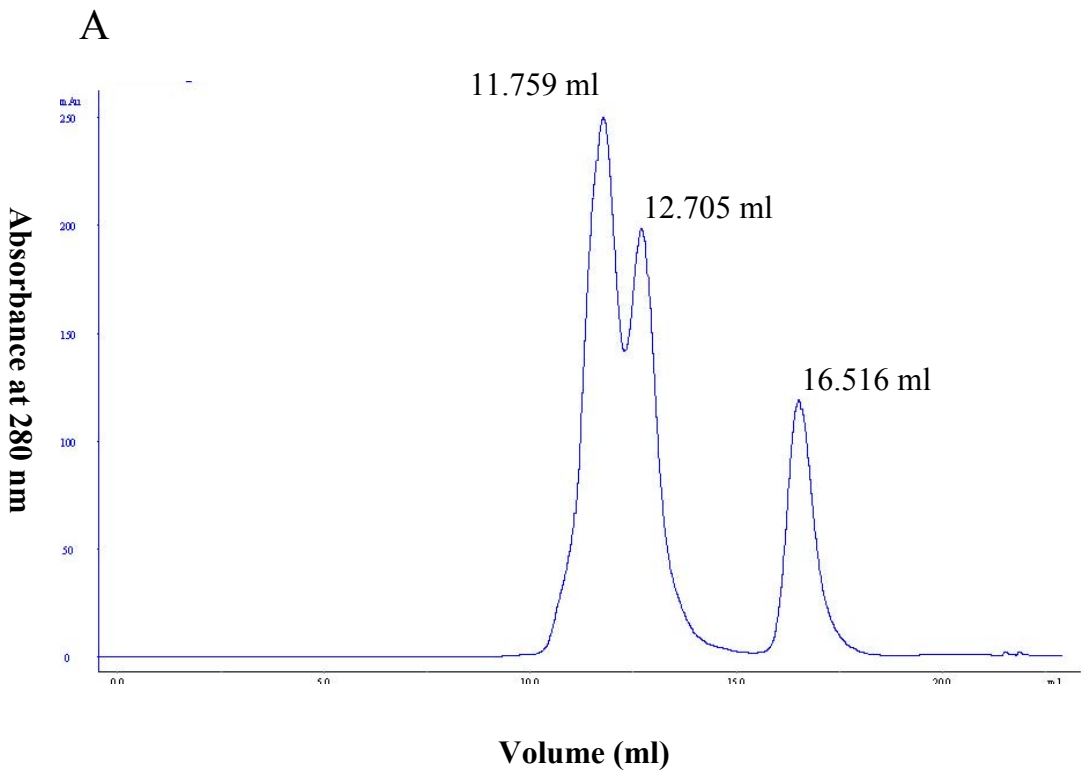

B

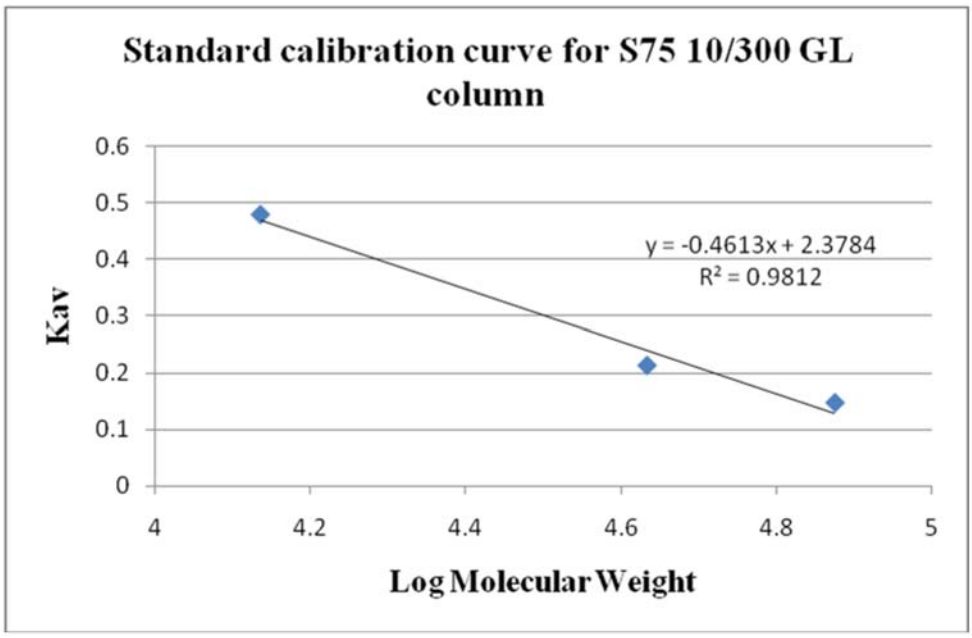

C

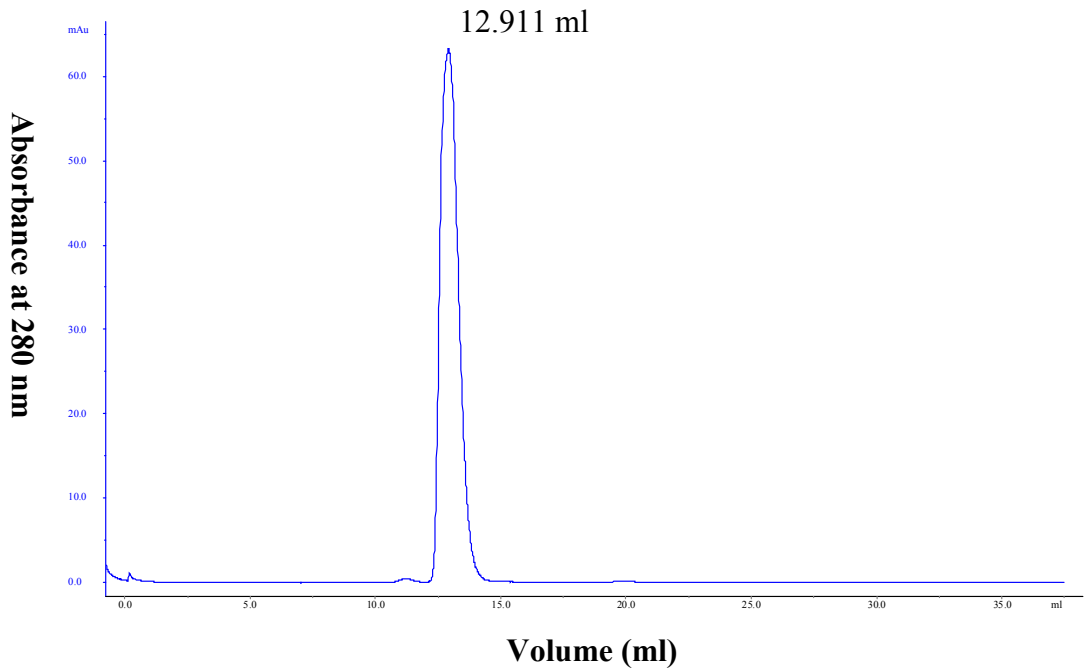

Figure 3.9. Gel filtration analysis of HutD. A. Chromatographic separation for the moleucular standards on S73 10/300 GL column. **B.** The stand calibration curve for the molecular standards. **C.** Chromatographic separation for HutD.

3.4 Crystallization of HutD

3.4.1 Initial crystallization trials

The His_6-HutD protein purified from Ni-NTA affinity chromatography was concentrated to ~20 mg/ml and the initial crystallization trial (480 crystallization conditions) was set up by using a medium-throughput robotic system (details see Section 2.12.1). Several small crystals (Figure 3.10) with the length of ~0.15 mm were observed in one environment (2.4 M ammonium formate, 0.05 M HEPES pH7.5) within the first few days.

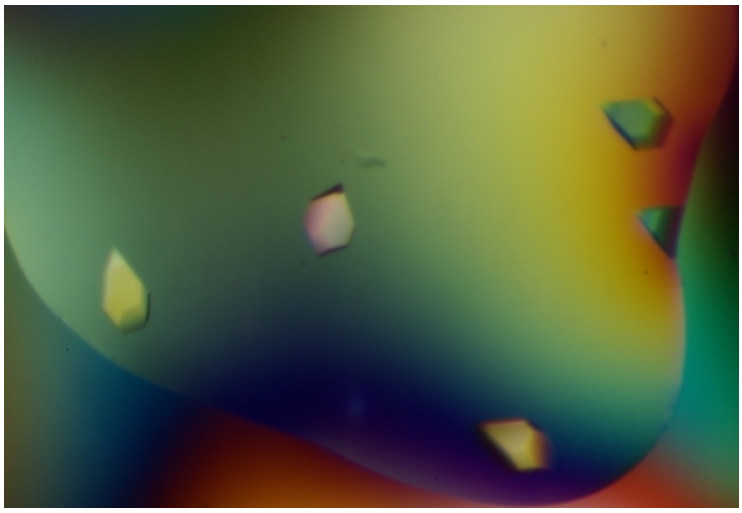

Figure 3.10. Initial crystallization of HutD. The crystallization trial containing a total of 480 conditions was set up for initial screens. The precipitant solution comprising 2.4 M ammonium formate, 0.05 M HEPES pH7.5 gave small HutD crystals.

3.4.2 Crystal optimization

To optimize the crystallization conditions, a fine screen around the promising condition were set up using 1 µl each of protein and precipitant solution in a 24-well sitting-drop plate (Section 2.12.2). The concentrations of ammonium formate varied from 1.6 M to 2.6 M, and HEPES from 0.05 M to 0.2 M (pH 7.5). Micro-crystals and needles were observed in 9 of the 24 conditions within the first five days. The crystals continued to grow and increased in size over three weeks and the largest crystals (~0.5 mm, Figure 3.11) were formed in two conditions (2.2 M ammonium formate, 0.2 M HEPES and 2.4 M ammonium formate, 0.2 M HEPES pH 7.5) (Figure 3.11).

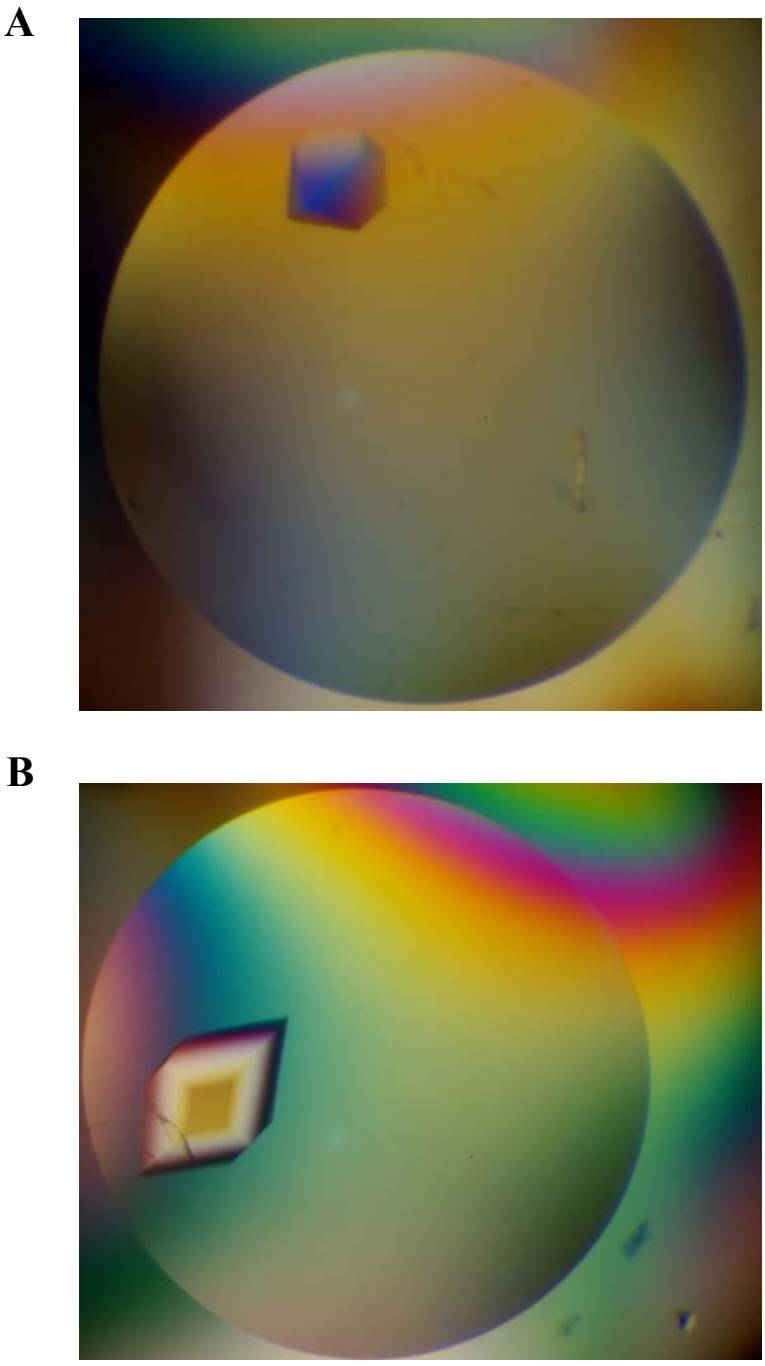

Figure 3.11. Optimization of crystallization conditions. HutD protein was screened against 24 various crystallization conditions. The larger crystals grew in two precipitant solutions (**A**: 2.2 M ammonium formate, 0.2 M HEPES pH 7.5; **B**: 2.4 M ammonium formate, 0.2 M HEPES pH 7.5).

3.5 Structure solution of HutD

3.5.1 Diffraction data collection and processing

HutD crystals were successfully formed in the precipitant solution (mother liquor) containing 2.2 M ammonium formate and 0.2 M HEPES pH 7.5. Cryo-solution consisting of the mother liquor and an increasing concentration of glycerol was prepared and tested for cryoprotection ability (Section 2.13.1). The cryo-solution containing 15% glycerol could be used for cryoprotection as no ice rings were observed on the diffraction image. The large HutD crystal produced in the fine screen was sequentially soaked in the cryo-solution with an increasing concentration of glycerol from 5% to 15%. After soaking, the crystal was flash-cooled by liquid nitrogen and immediately subjected to X-ray exposure. The data of 200 diffraction images were collected with 1° oscillation angle at low resolution to 2.99 Å while another dataset of 200 images for higher resolution (up to 1.79 Å) were collected using the same conditions but a shorter detector-to-crystal distance. The crystal was exposed to X-ray for 150 seconds per image. The two datasets were processed in *Denzo* (Otwinowski and Minor, 1997), which suggested that the possible Bravais lattice for the HutD crystal was primitive tetragonal. The data were subsequently scaled using *Scalepack* (Otwinowski and Minor, 1997) in $P4_1$, $P4_12_12$ and relative space groups. The statistics χ^2 value and I/σI for reflections expected to be absent in certain space group were examined. P422, $P4_12_12$ and $P4_32_12$ were shown to be possible correct space groups since they had acceptable χ^2 values and the reflections expected to be absent had small I/σI values.

3.5.2 Number of molecules in the asymmetric unit

To estimate the number of molecules in the asymmetric unit, the Matthews coefficient was calculated in the CCP4 programme (Bailey, 1994). The most likely value was 3.52 $Å^3$/Da, corresponding to 2 molecules per asymmetric unit and 65.08% solvent content.

3.5.3 Phase determination by molecular replacement

Molecular replacement (MR) enables the solution of the phase problem where a known protein structure shares ~35% or higher sequence identity with the unknown

protein (Schwarzenbacher et al., 2004). As blastp (protein-protein BLAST) search using the deduced amino acid sequence of *hutD* shows that it shares 54% identity with the conserved hypothetical protein PA5401 from *Pseudomonas aeruginosa* PAO1 whose structure has been solved (PDB ID: 1yll), MR via the programme Phaser (McCoy, A. J., 2007) was used to solve the HutD structure. The programme Chainsaw (McCoy et al., 2007) via the CCP4 interface (Bailey, 1994) was performed to truncate non-conserved resides in PA5401 to the gamma carbon. The modified PA5401 pdb file was used as a search model for MR and the possible space groups (P422, $P4_12_12$ and $P4_32_12$) were examined in Phaser. After the rotation function and the translation function were carried out, the orientations of the asymmetric unit were scored with the Log Likelihood Gain (LLG) and the Z-score. The LLG measures how much better the data can be predicted from the oriented model than from a random distribution of the same atoms. The Z-score is the number of standard deviations above the mean for a particular LLG (McCoy et al., 2007). The space group of HutD crystal was reported as $P4_12_12$ with a single solution. The increasing and positive LLG (from 313 to 1355) and high TFZ (Translation Function Z-score, TFZ = 26.8) suggest this was the correct structure solution for the HutD crystal. The data collection and processing statistics are summarized in Table 3.1.

Table 3.1. A summary of processing statistics of HutD crystal

	HutD
Space group	$P4_12_12$
Cell dimension (Å)	a=82.86; b=82.86; c=174.42
Resolution range (Å)[a]	50.0 – 1.79 (1.85 – 1.79)
No. of observed reflections	534919
No. of unique reflections	57509
$\boldsymbol{R_{merge}}$ **(%)**[a,b]	3.7 (29.0)
Mean I/σI [a]	58.7 (6.26)
Multiplicity [a]	9.3 (6.9)
Completeness (%)[a]	98.9 (88.7)

[a] Values in parentheses are for the outermost shell of data

[b] $R_{merge} = \sum_h \sum_j | I_{jh} - (I_h) | / \sum_h \sum_j (I_h)$

where I_{jh} is the intensity of the jth observation of reflection h

(I_h) is the mean intensity of all observations of reflection h.

3.5.4 Model building, refinement and quality assessment

The HutD structure solution of molecular replacement was refined in Refmac (Murshudov et al., 1997) using restrained refinement with a weighting term (relating reflection data and geometry restraints) of 0.5. Electron density maps displayed in Coot (Emsley and Cowtan, 2004) were used for model building. The model was built into a SigmaA-weighted 2|Fo|-|Fc| density map contoured at 1-1.5 σ and a SigmaA-weighted |Fo|-|Fc| difference map contoured at 2.5-3.5 σ. The modified model containing new entities such as altered amino acids and water molecules was subsequently refined in Refmac. During refinement, the values of R and R_{free} were examined to evaluate the quality of process. The model building and refinement resulted in a decrease in both R and R_{free} values from 23.47% and 25.76% in the initial model to 19.04% and 21.98% in the final model. The drop of R and R_{free} indicates the success of refinement. Also, the built-in tools in Coot were used to quickly analyze the geometry and rotamer of amino acids, density fit, position of water molecules and a Ramachandran plot during the refinement. The final model was composed of residues 3-186 for chain A, residues 2-34 and 37-186 for chain B, 1 glycerol molecule, 27 formates and 276 water molecules. The high-quality electron density map was lacking for the attached poly-histidine tag, several residues at N-terminus in each chain and 2 residues for a loop in the chain B. The final model was validated using Molprobity (Davis et al., 2007) and the Ramachandran plot (Figure 3.12) shows that 1.3% of all residues are in allowed region while 98.7% of them are in favoured region. The refinement and model statistics are given in Table 3.2.

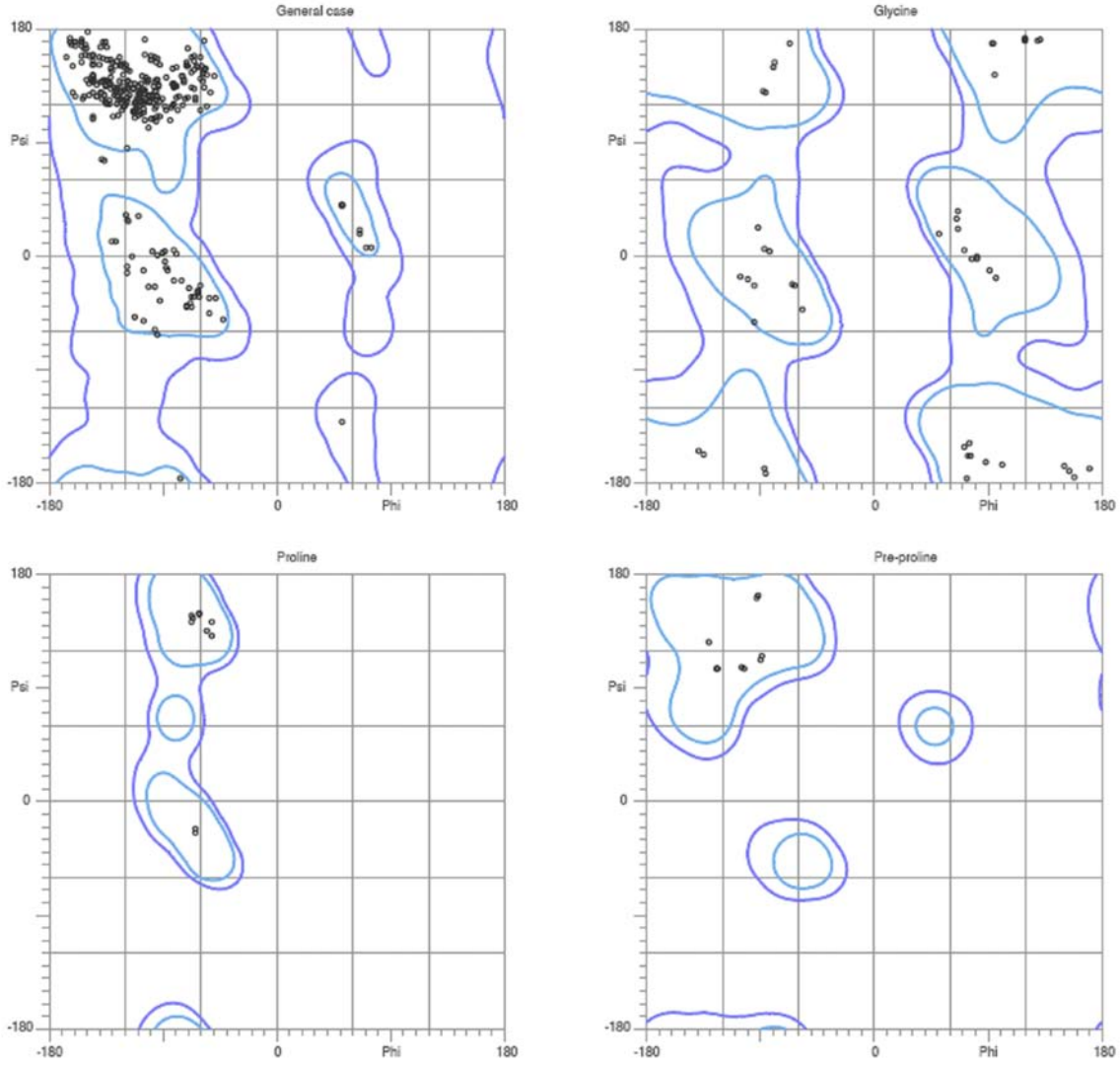

Figure 3.12. Ramachandran plot for the final model of HutD. The plot is generated by Molprobity and no outliers are observed. The outline in light blue and dark blue represents the favoured and allowed regions.

Table 3.2. Summary of refinement and model statistics.

Resolution range (Å)	43.60 – 1.80
No. of reflections	54475
R-factor (R_{free}) (%)	19.3 (22.3)
Model details	
No. of protein atoms	2844
Other molecules	1 glycerol, 27 formates
No. of water molecules	276
rms deviations	
Bond lengths (Å)	0.017
Bond angles (deg.)	1.47
Wilson B factor ($Å^2$)	25.88
Mean B factors ($Å^2$)	25.89
Ramachandran plot	
Favoured regions (%)	98.7
Allowed regions (%)	1.3

3.6 Description of HutD structure

3.6.1 Overall topology of HutD structure

The asymmetric unit of the crystal contains two monomers (Chain A and Chain B) and PISA (Protein Interfaces, Surfaces and Assemblies) (Krissinel and Henrick, 2007) analysis of HutD structure showed that these two monomers could form a dimer. The buried surface area for Chain A and Chain B is 665.4 $Å^2$ and 686.6 $Å^2$ respectively which corresponds to 7.0% and 7.4% of each monomer. A number of hydrogen bonds detected at the interface are important for the formation of the dimer. The HutD dimer is rod-shaped (Figure 3.13) and each monomer is folded into two major domains (Domain I and II) and one subdomain (Figure 3.14). The subdomain is made up of one-stranded β-sheet (S1) and one α-helix (H1) while the two domains that are barrel-shaped are composed of only antiparallel β-sheets, with ten strands for Domain I (S2 – S11) and eight strands for Domain II (S12 – S19). These two domains are connected by a loop (between S11 and S12) comprising 7 residues. The two-stranded antiparallel β-sheet (S12 and S13) might form a crucial part of the interaction between monomers in the dimer.

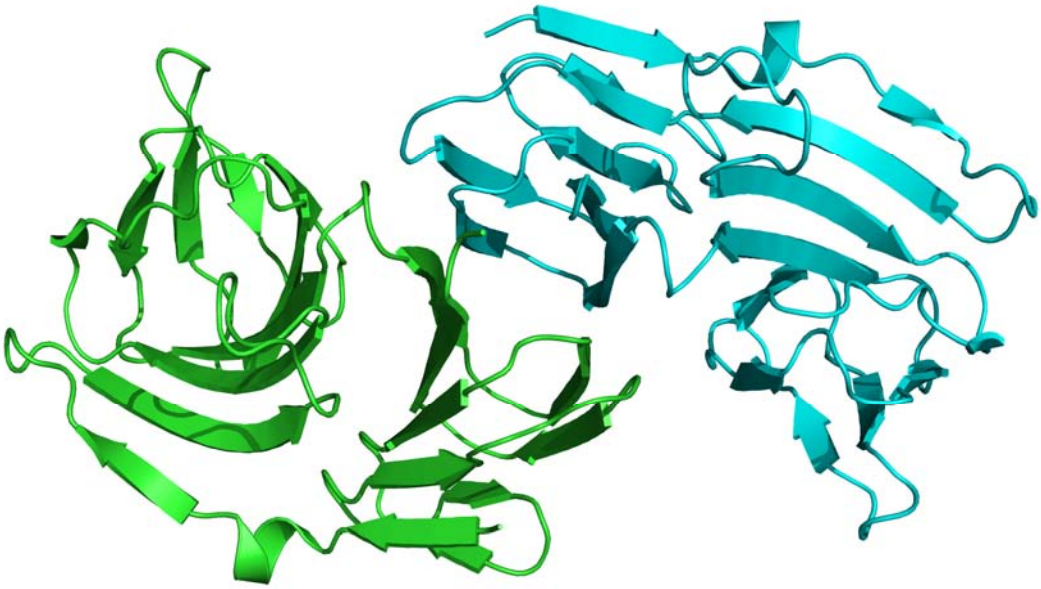

Figure 3.13. Cartoon representation of HutD dimer. The cartoon diagram of HutD dimer is drawn using PyMOL. Chain A is coloured in green and chain B is coloured in blue.

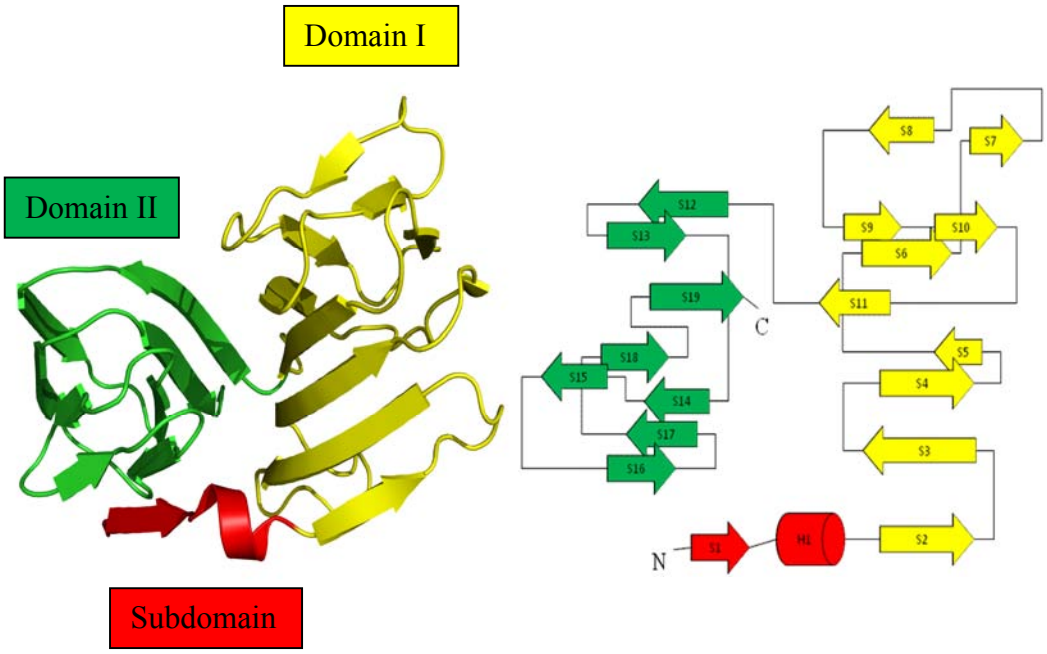

Figure 3.14. Cartoon representation (A) and topology diagram (B) of HutD monomer. Two β-barrel domains are shown as yellow (domain I) and green (domain II), respectively. The subdomain is coloured in red. The cartoon representation of HutD monomer was drawn using PyMOL.

3.6.2 Structural comparison of HutD monomer

The structure of HutD monomer was compared with other protein structures in the Protein Data Bank (PDB) using a Dali search (Holm, et al., 2008). It revealed seven protein structures with Z-score greater than 14. Comparison of HutD monomer with protein structures in the PDB using Secondary Structure Matching (SSM) (Krissinel and Henrick, 2004) displayed eight structures with Z-score greater than greater than 5. The Dali and SSM structural matches are listed in Table 3.3. These proteins are the members of RmlC-like cupins superfamily. The similar structure shared by these proteins and HutD is described as double-stranded beta-helix in SCOP (Murzin et al., 1995), but their function are still unknown.

Table 3.3. Structural similarity of HutD monomer found using Dali and SSM

Structure	Z-score	r.m.s. deviation
Conserved hypothetical protein PA5104 from *P. aeruginosa* PA01	27.0 (11.3)[a]	1.4 (1.12)[a]
Pirin-like protein GK1651 from *G. kaustophilus*	16.0 (6.1)	2.8 (2.35)
Protein Yhhw from *E. coli*	15.9 (7.5)	2.5 (2.33)
Conserved hypothetical protein DR1152 from *D. radiodurans* R1	15.1 (7.2)	2.7 (2.33)
Hypothetical protein Ylba from *E. coli*	14.9 (5.1)	2.8 (2.60)
Glyoxylate induced protein from *P. aeruginosa*	14.5 (6.2)	2.6 (2.36)
Cupin domain protein EF2296 from *E. faecalis*	14.2	2.9
Quercetin 2,3-dioxygenase from *A. japonicus*	(7.2)	(2.43)
Human pirin	(5.5)	(2.70)

[a] Values in parentheses are for the Secondary Structure Matching (SSM) data

As comparison of three-dimension (3D) structures of proteins may reveal biologically interesting clues as to their functions, the ConSurf server (Landau et al., 2005) which is able to identify the functionally important regions of a protein of known 3D structure was carried out for the HutD structure. A conserved region is observed on the surface of HutD and a pocket consisted of conserved residues is found in the β-barrel domain (Red area) (Figure 3.15A). These conserved regions are only found in the Domain I (Figure 3.14). By examining the highly conserved residues around the putative binding pocket, the side chains of aspartic acid (Asp108), asparagine (Asn110) and arginine (Arg61) which protrude toward the inside of β-barrel domain may enable the formation of hydrogen or ionic bonds with ligands (Figure 3.15B).

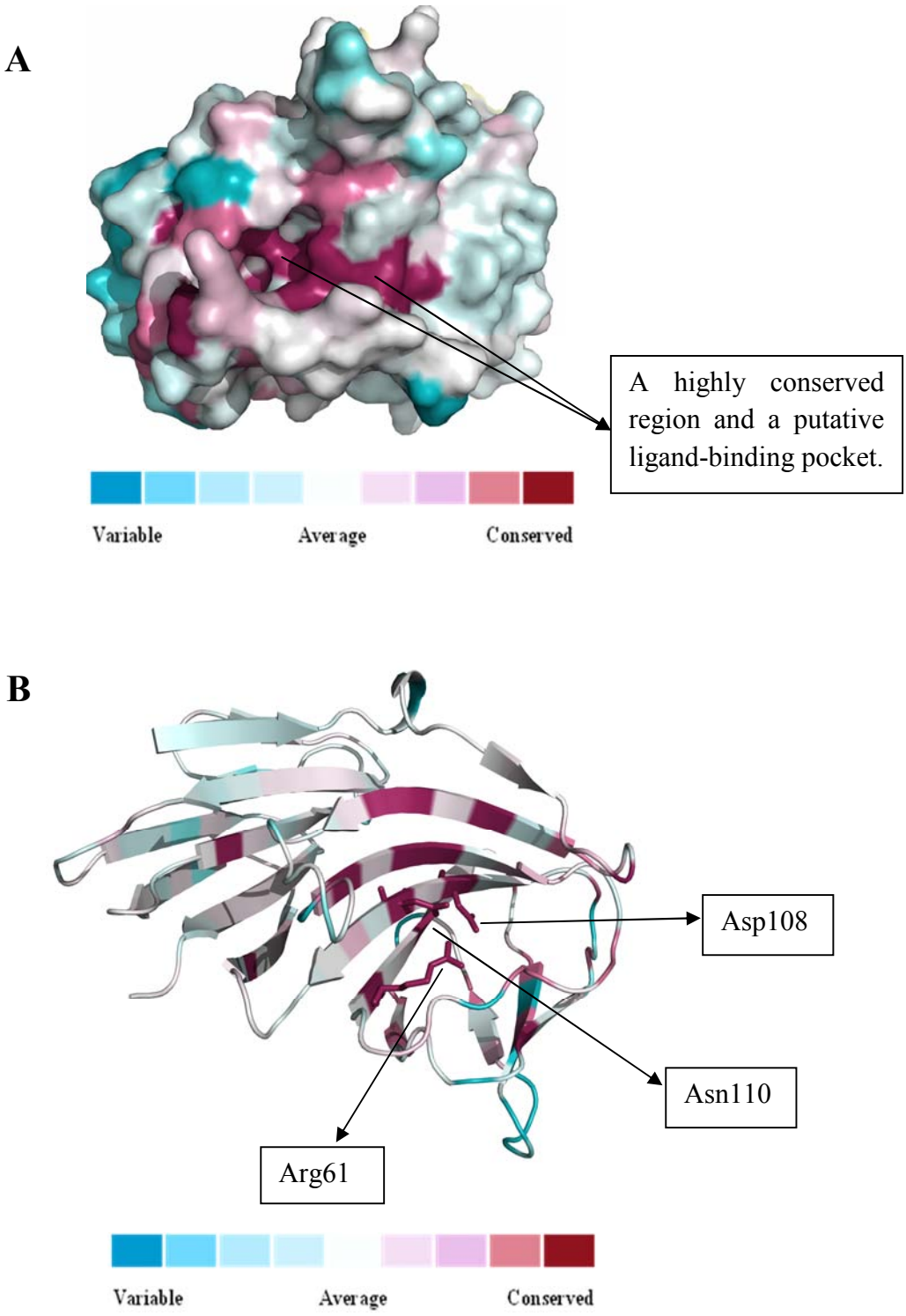

Figure 3.15. Conservation pattern obtained using ConSurf for HutD. HutD is presented as surface (**A**) and cartoon model (**B**), and coloured according to the conservation scores.

Next, the ConSurf search for HutD homologues was restricted to *Pseudomonas* species. The putative ligand-binding pocket was still observed and additional conserved regions around the pocket were also detected (Figure 3.16). Conserved residues are mainly located into three sequence clusters corresponding to residues 15-28 (cluster 1), residues 41-71 (cluster 2) and residues 106-115 (cluster 3). Interestingly, one formate and one glycerol (contained in precipitant solution) detected in the putative binding pocket interact with several conserved residues (Asn19, Ser54, Arg61, Asp108 and Asn110) (Figure 3.17). The formate forms salt-bridges to Arg61 and Asn110. Hydrogen bonding interactions occur among the formate, Asp108, Asn110 and water. The glycerol interacts with Asn19 and Ser54 via a salt-bridge and a hydrogen bond. Taken together, the observation of the putative pocket and the conserved area on the surface of HutD suggests that small molecules or other proteins may interact with HutD.

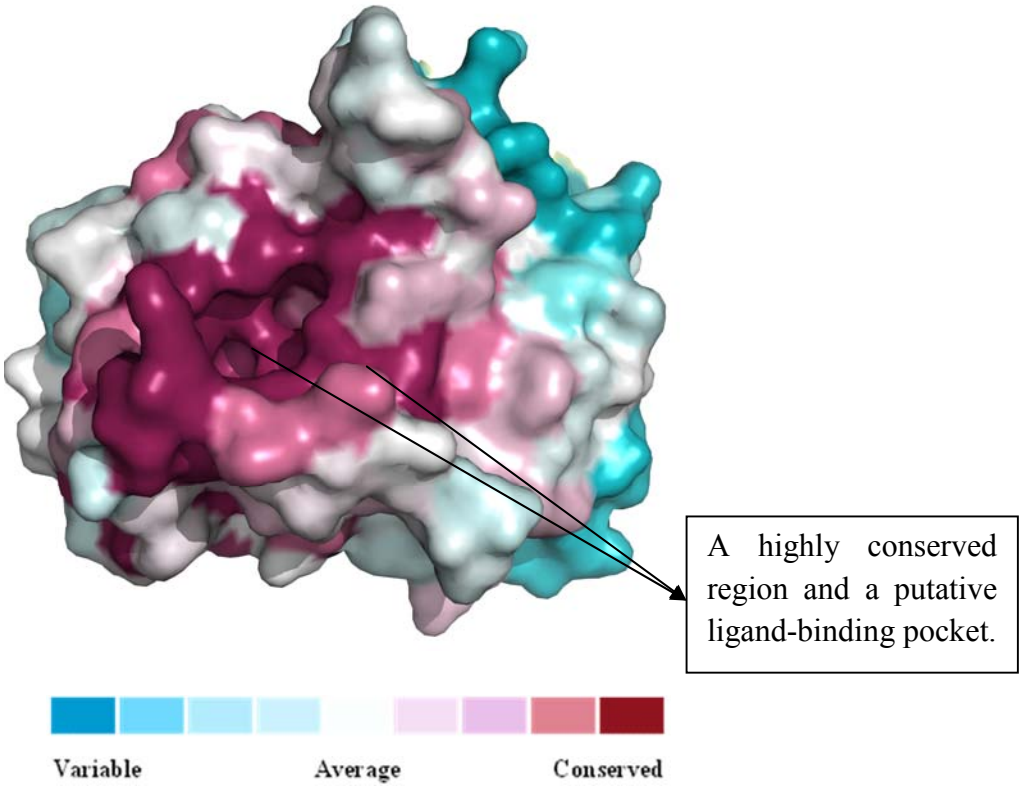

Figure 3.16. Conservation pattern obtained using ConSurf for HutD in *Pseudomonas*. The HutD is presented as surface model, and coloured according to the conservation scores.

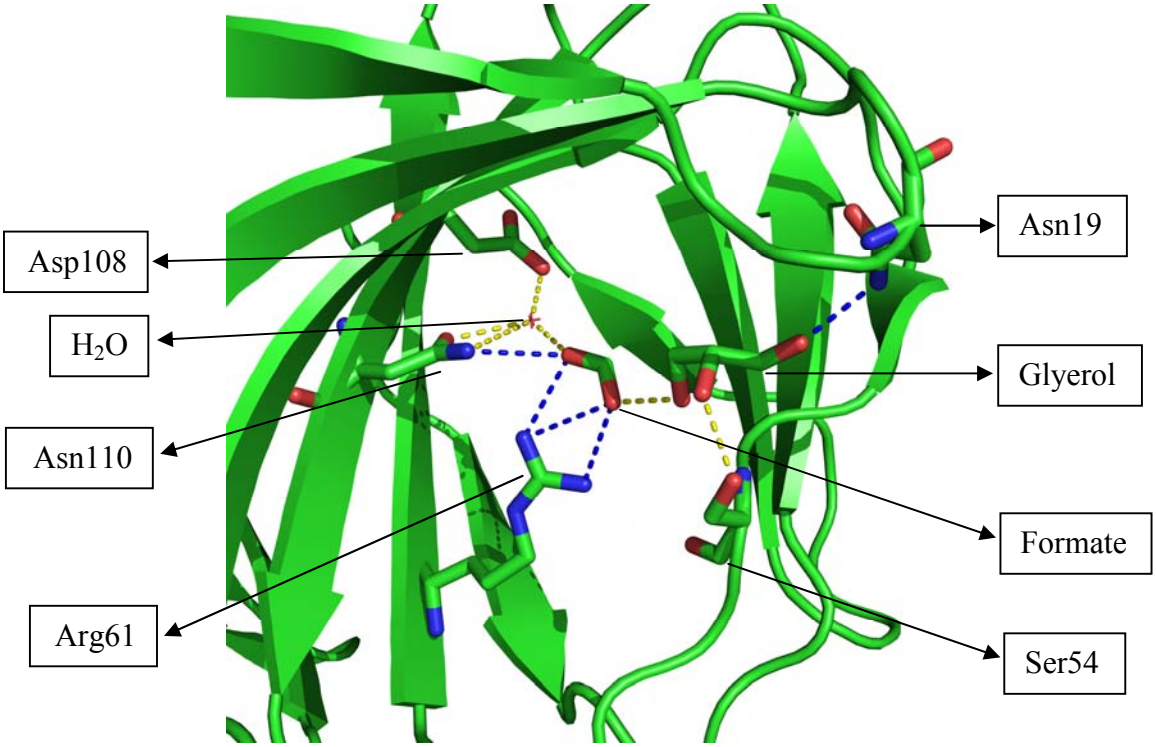

Figure 3.17. Cartoon representation of putative binding pocket. Highly conserved residues (Asn19, Ser54, Arg61, Asp108 and Asn110) are shown as stick models using PyMOL. Salt-bridges are drawn as blue broken lines and hydrogen bonds are shown as yellow broken lines, respectively.

3.7 Protein functional tests

The *hut* operon is negatively regulated by the repressor HutC and is derepressed through the interaction of HutC with an inducer urocanate. The hypothesis is that HutD could bind to urocanate and therefore limit the expression level of *hut* operon by controlling the intracellular concentration of urocanate. The interaction between HutD and putative ligands (histidine and urocanate) was studied by two methods: thermal shift assay and isothermal titration calorimetry.

3.7.1 Thermal shift assay

Thermal shift assay is a rapid screening method to detect interaction between ligands and proteins (details see Section 2.11.1). The proteins are subjected to gradually increasing temperature in the presence of a fluorescent dye. The fluorescent dye binds to the hydrophobic sites of denatured proteins and emits fluorescent signals. The melting temperature (Tm), at which the concentrations of folded and unfolded protein are equal, is measured in the assay. If ligands bind and stabilize proteins, it may cause an increase in the melting temperature of proteins (Niesen et al., 2007). The interaction of HutD with ligands (histidine and urocanate) was explored. Before conducting the thermal shift assay, four different concentrations of HutD (from 50 µg/ml to 200 µg/ml) were used to determine the suitable concentration for the assay. 100 µg/ml of HutD was selected for the subsequent thermal shift assay as it generated a strong fluorescent signal at relatively low concentration (Figure 3.18).

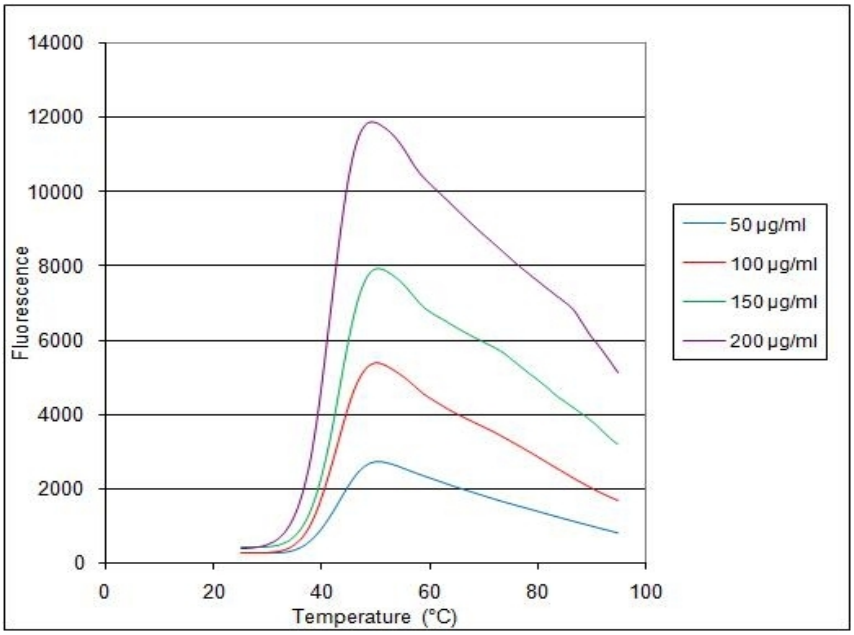

Figure 3.18. Recording of fluorescence internsity for different concentrations of HutD. 50 µg/ml, 100 µg/ml, 150 µg/ml and 200 µg/ml of HutD were used to determine the suitable concentration of HutD for the thermal shift assay.

To set up thermal shift assay, HutD was placed into wells of a 96-well plate in the presence of SYPRO orange and various concentrations of histidine or urocanate. The plate was heated from 25ºC to 95ºC and the fluorescent signal was recorded (Figure 3.19, A and B). The observed Tm of HutD in the absence of histidine was 40.7 ± 0.3ºC and it was 41.3 ± 0.3ºC in the absence of urocanate. There was a gradual increase in the observed Tm in the presence of histidine or urocanate (Figure 3.19, C and D). The melting temperature of HutD was increased by approximately 14ºC when 50 mM of histidine or urocanate was added. These results suggest that HutD could be stabilised by both histidine and urocanate; however, the interaction between them was quite weak since the saturable binding was observed only at high concentration of ligands.

A

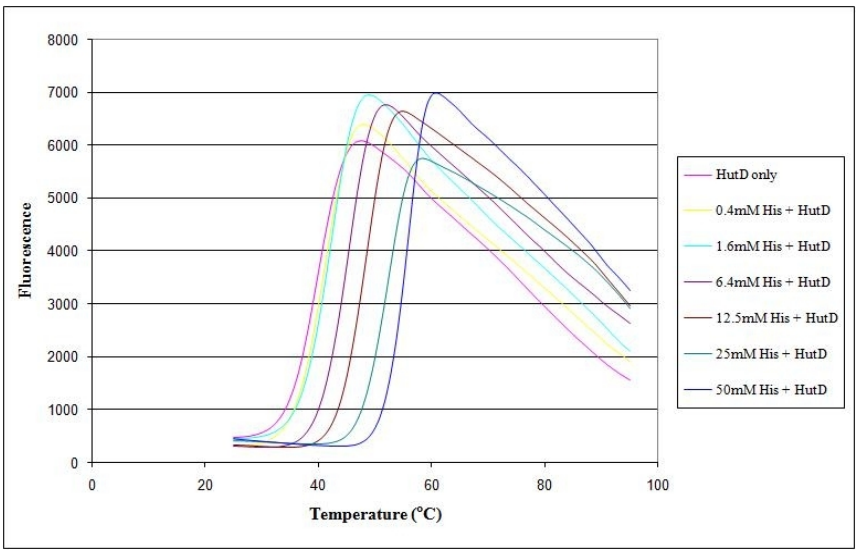

B

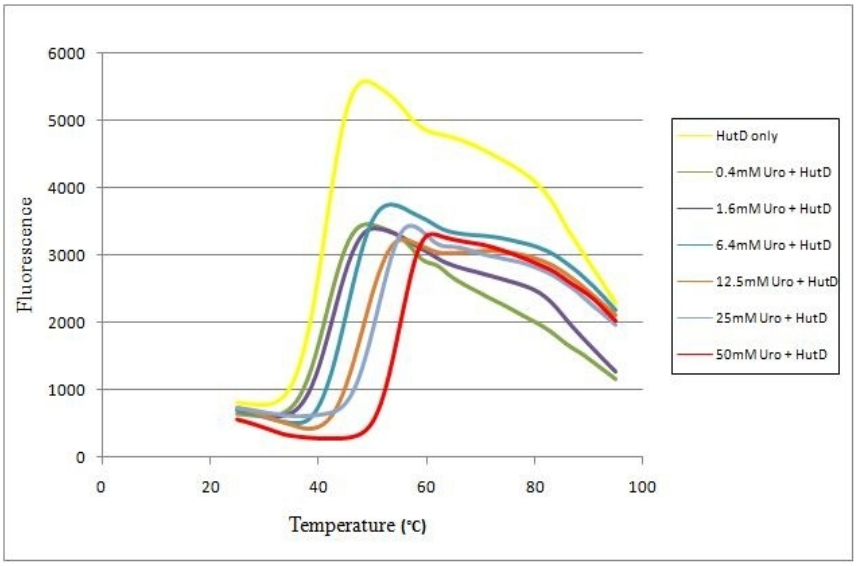

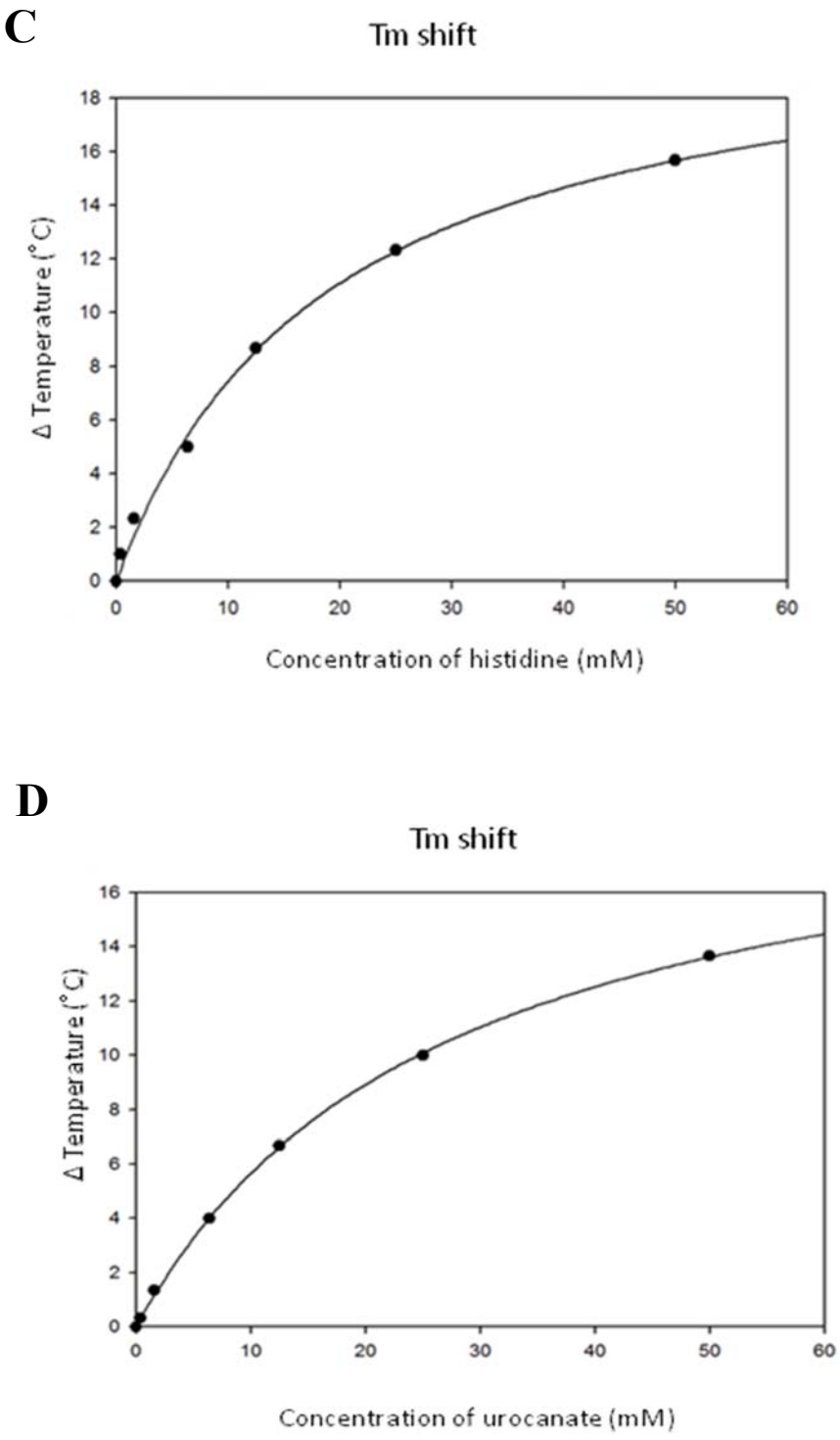

Figure 3.19. Analysis of interaction of HutD with histidine (his) and urocanate (uro). The thermostability of HutD in the presence of 0, 0.4, 1.6, 6.4, 12.5, 25 and 50 mM histidine (**A**) or urocanate (**B**) was measured by thermal shift assay. The increase of ΔTm in the various concentration of histidine (**C**) or urocanate (**D**). The data in panels C and D were processed with SigmaPlot10.

3.7.2 Isothermal titration calorimetry

Thermal shift assay examines the effect of ligands on the stability of proteins and its ability to provide estimates of protein-ligand binding activity is limited (Niesen et al., 2007). Isothermal titration calorimetry (details see Section 2.11.2), which directly explores the thermodynamics of biomolecular interactions, was performed to study the interaction between HutD and putative ligands (histidine and urocanate).

Initially, both purified HutD and histidine (or urocanate) were dialysed against a large volume of same buffer (20 mM HEPES pH7.5 and 150 mM NaCl) as used for protein storage. It is crucial that the composition of solutions containing proteins and ligands is identical as the difference in pH, buffer or salt concentration will generate heat of dilution signals that could mask the heat signals produced by the actual binding reaction. After dialysis, the concentrations of proteins and ligands were determined by UV absorbance analysis (the final ITC analysis depends on their accurate concentrations (Freyer and Lewis, 2008)).

The interaction between HutD and histidine was firstly examined. 28 injections of 22.78 mM histidine (in the syringe injector) were delivered into 12 μM of HutD (in the sample cell). A control experiment was performed by injecting histidine into the buffer (dialysate) (Figure 3.20A). The raw ITC data show an exothermic heat pulse on each injection and a gradual decease in the peak of heat on subsequent injections (Figure 3.20B). The raw data were corrected for heat of dilution effects and the curve of integrated heat peaks against the molar ratio was plotted. Random scattered data points were observed and were fitted into a flat line (Figure 3.20C). These results suggest that histidine could not specifically bind to HutD. Next, the interaction between HutD and urocanate was studied. 35 μM of HutD in the cell was titrated with 53.23 mM of urocanate and a control experiment in which urocanate was injected into buffer was also carried out. An endothermic reaction between HutD and urocanate was observed (Figure 3.21B). The integrated heat data were fitted with a one-site binding model (Figure 3.21C). The binding of urocanate is driven by a negative enthalpy change (ΔH) of -2.71 kcal/mole with a dissociation constant (K_D) of 5.6 mM. The high dissociation constant derived from the ITC experiment suggests a weak interaction between HutD and urocanate.

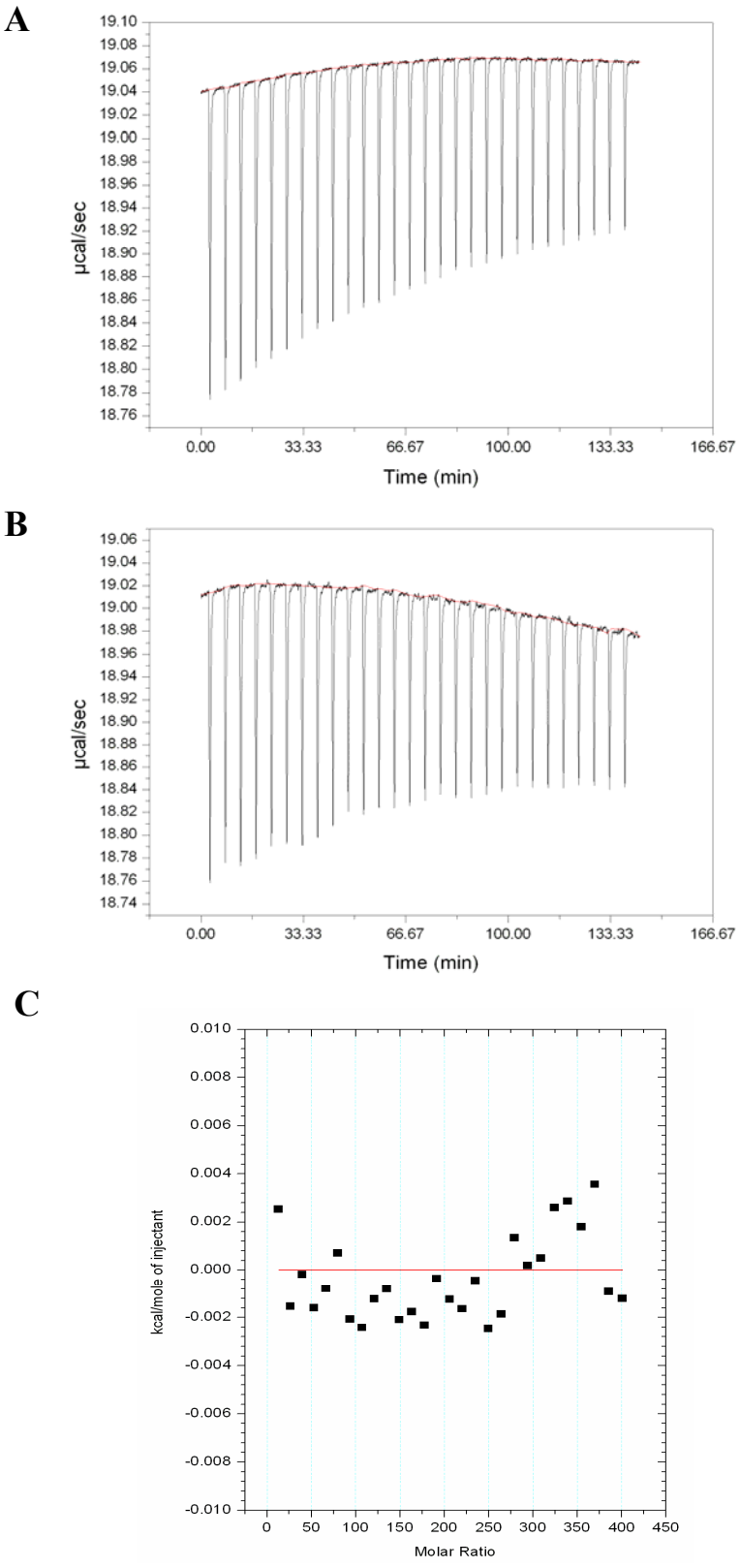

Figure 3.20. Isothermal titration calorimetry of histidine and HutD. A: the control experiment (histidine-to-buffer) for ITC. **B:** Raw data for titration of 12 µM of HutD with 22.78 mM histidine. **C:** Integrated heat data (heat of dilution corrected) with a fit model. All ITC experiments were carried out in 150 mM NaCl and 20 mM HEPES pH 7.5 at 20ºC.

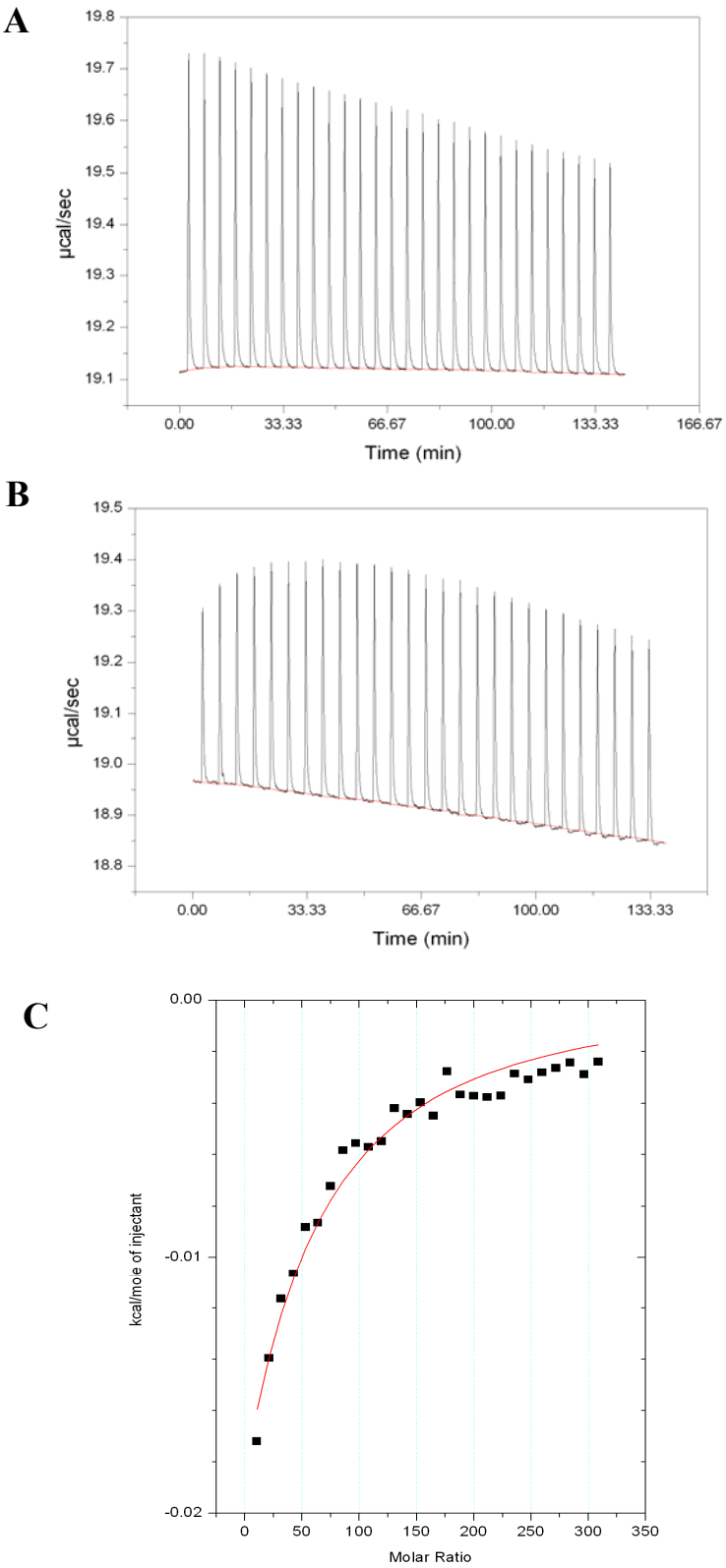

Figure 3.21. Isothermal titration calorimetry of urocanate and HutD. A: ITC control experiment (urocanate-to-buffer). **B:** Raw data for titration of 35 µM of HutD with 53.23 mM urocanate. **C:** Integrated heat data (heat of dilution corrected) with a fit model. All ITC experiments were carried out in 150 mM NaCl and 20 mM HEPES pH 7.5 at 20ºC.

Discussion

4.1 The effect of growing temperature on HutD preparation

HutD was successfully overexpressed in *E. coli* at 37ºC; however, a large amount of HutD was insoluble in cells grown under this temperature. The protein expression in host cells is usually influenced by various growth factors such as temperature, inducer concentration, induction time and duration (Donovan et al., 1996). We examined the effect of growth temperature on HutD solubility. Our results showed a large effect of growing temperature on protein solubility: when HutD was induced at 25ºC instead of 37ºC, a large proportion of HutD was soluble. The effect can be explained by the possibility that high temperatures could enhance interaction of hydrophobic regions of protein folding intermediates and promote the formation of inclusion bodies (Mitraki and King, 1989), whereas lower growth temperatures may reduce the expression rate of unfolded proteins and decrease the kinetics of protein intermediate interaction, and thus limit the aggregate formation and enhance the protein solubility.

4.2 Determination of molecular weight of HutD

Although the predicted molecular weight of HutD is 21.2 kDa, it is curious to show that the molecular mass of HutD is repeatedly lower than the 20 kDa marker in the SDS-PAGE analysis. The size-exclusion chromatography was performed to determine the molecular weight of HutD. HutD elutes from the gel filtration column at 12.911 ml, which suggests that native state HutD is smaller than the 43.0 kDa molecular standard (Ve = 12.705 ml). However, the estimated molecular weight of HutD is 45.8 kDa using standard calibration curve. This opposite conclusion may be caused by the inadequate molecular standards used in the size-exclusion chromatography. More molecular standards should be used to accurately determine the molecular mass of HutD.

4.3 Comparative structural analysis of HutD

The deduced amino acid sequence of SBW25 *hutD* shares 54% identity with the conserved hypothetical protein PA5401 from *Pseudomonas aeruginosa* PAO1, whose structure is currently available. Molecular replacement was thus performed to solve

the structure HutD from *P. fluorescens* SBW25 based on the X-ray data. The HutD monomer is consisted of two β-barrel domains and a subdomain. The comparative structural analysis of HutD indicated it belongs to the RmlC-like cupin superfamily. Although it contains similar β-barrel structures HutD does not have two conserved sequences of the cupin superfamily, namely $GX_5HXHX_{3,4}EX_6G$ and $GX_5PXGX_2HX_3N$ separated by a variable stretch of amino acids. These motifs are required for metal ion binding (Pang et al., 2004; Adams and Jia, 2005). However, comparison of three-dimension structure of HutD with the close homologues of known protein structures showed a putative binding pocket located in the β-barrel domain and a conserved region on the surface of HutD. The side chains of highly conserved aspartic acid (Asp108), asparagine (Asn110) and arginine (Arg61) that are able to form weak interactions protrude toward the inside of β-barrel domain. The putative binding pocket and conserved residues are still detected when searching HutD structural homologues from *Pseudomonas*. Interestingly, a formate molecule forms salt-bridges to the conserved Arg61 in the putative binding pocket. These data suggest that small molecules having functional carboxylic group(s) may interact with HutD and the conserved residues (Asp108, Asn110 and Arg61) in the pocket structure may be candidates for ligand binding sites.

Structure comparison is a powerful tool for the discovery of evolutionary relationships or homology that is hidden at the primary sequence level (Thornton et al., 2000). Although numbers of structures are available in the in the Protein Data Bank, there is evidence to suggest that there is a finite number of protein folds (Orengo et al., 1999). Comparison of the protein fold or motif with those of other proteins may reveal the biochemical function of the protein. A typical example is the helix-turn-helix motif that is formed in proteins that bind DNA. However, different biochemical functions of proteins have been found even though they share the same fold (Thornton et al., 2000). In this study, little insight into the molecular mechanism of HutD action has emerged from structure comparison even though HutD has a number of features including common β-barrel domains. In order to further elucidate HutD function it will be necessary to put forward a hypothesis as to likely function that can be tested using biochemical approaches.

4.4 Function of HutD

The *P. fluorescens* SBW25 HutD contains a putative pocket structure, suggesting that HutD functions by binding to small molecules. Here we performed thermal shift assay and isothermal titration calorimetry (ITC) analysis to test the interactions between HutD and two putative ligands, histidine and urocanate. The result of thermal shift assay suggested a weak binding of HutD to both histidine and urocanate with a saturation concentration at 50 mM. However, the ITC data suggested a weak binding to urocanate only. This disagreement could result from the limitation of the thermal shift assay. There is an assumption that ligands only interact with the native state of a protein but not with the unfolded state (Lo et al., 2004). The ΔT_m shift in the presence of histidine may be caused by the non-specific binding between histidine and unfolded HutD when denaturing HutD by heating in the thermal shift assay. Furthermore, another assumption of this method is that the thermal denaturation of proteins follows a two-state reversible mechanism. However, the thermal unfolding process is irreversible for many multidomain proteins (Pantoliano et al., 2001; Niesen et al., 2007).

Isothermal titration calorimetry directly detects the thermodynamics and kinetics of the interaction between biological molecules. The resulting data indicated that urocanate was weakly bound to HutD but the interaction between histidine and HutD was not detectable. A one-site binding model for the urocanate-HutD interaction was generated and the dissociation constant was determined to be 5.6 mM. The enthalpy change (ΔH) estimated to be -2.71 kcal/mole from the model implies an exothermic reaction (heat release) between HutD and urocanate. However, the raw ITC data indicate an endothermic reaction (heat absorption). In the ITC experiment, the raw data display the mean heat (Q_{mean}) which includes the heat generated from ligand-to-protein titration ($Q_{ligand,protein}$) and heat produced from ligand-to-buffer titration ($Q_{ligand,buffer}$; the control). Because of heat of dilution for ligands, these data are corrected by subtracting heat of the control from the mean heat ($Q_{ligand,protein} = Q_{mean} - Q_{ligand,buffer}$), and are subsequently used for model fitting (Freyer and Lewis, 2008). The possibility of the difference between raw ITC data and model fitting data could be that the heat of the control (urocanate-to-buffer) masked the heat of urocanate-to-HutD titration. The reaction of urocanate-to-buffer was endothermic while the

interaction of urocanate-to-HutD might be exothermic. The magnitude of heat of urocanate-to-HutD titration was smaller than that of urocanate-to-buffer titration and hence the mean heat data display an endothermic reaction while the corrected data indicated an exothermic reaction.

The low heat signal for the urocanate-to-HutD titration may result from the impurity of urocanate. It has been shown that there are two isomers of urocanate: *cis*- and *trans*-urocanic acid (UCA). Conversion of *trans*-UCA to *cis*-UCA is mediated by UV radiation, i.e. exposure to sunlight or incandescent lamp light. Importantly, window glass could not prevent the urocanate photoisomerization (Hug and Hunter, 1994). Only *trans*-UCA can be metabolized by the *hut* enzymes. It is highly possible that our urocanate samples contain a larger proportion of *cis*-UCA. This can explain why binding signal was very weak even at high urocanate concentration (53.23 mM). Because of low concentration of *trans*-UCA, the heat generated from the exothermic reaction between HutD and *trans*-UCA could be quite low and overwhelmed by the heat of dilution for urocanate.

Recent ITC analysis by Dr Monica Gerth has shown that HutD from *P. aeruginosa* PAO1 binds to N-formylglutamate (FG). Also, HutG can be weakly induced by FG (Hu et al., 1989). This suggests that HutD may bind to the weak promoter region of *hutG* and repress its expression. If the hypothesis of HutD binding to urocanate is finally rejected, the ability of HutD binding to FG and other intermediates of the *hut* catabolic pathway in *P. fluorescens* SBW 25 should be tested.

Conclusion and Future Studies

HutD is a broadly conserved but functionally unknown component of the histidine utilization pathway in *Pseudomonas*. Genetic and fitness analysis of *hutD* in a plant-growth promoting bacterium *P. fluorescens* SBW25 indicated that *hutD* plays a regulatory role in expression of the *hut* enzymes but the molecular mechanisms of HutD action remains unknown. This work aims to express the *P. fluorescens* SBW25 HutD in *E. coli*, determine the 3-D crystal structure of HutD and test one of the hypotheses that HutD functions via specific binding to urocanate.

HutD expression: The HutD gene of *P. fluorescens* SBW25 has been successfully cloned and expressed in *E. coli*. Growth at low temperature (25 ºC) was shown critical to prepare soluble HutD at large scale.

Multimerization state of HutD: Analytic size-exclusion chromatography showed that HutD forms a dimer in the elution buffer.

Crystallization of HutD: Large crystals (~ 0.5 mm) were obtained and X-ray diffraction data was collected at a resolution level up to 1.79 Å. The 3-D structure was then solved by molecular replacement with the HutD from *P. aeruginosa*. The SBW25 contains two molecules in an asymmetric unit (Chain A and Chain B) and each monomer is composed of one subdomain and two β-barrel domains. Comparative structural analysis indicates a putative binding pocket in the Domain I and a conserved region on the surface of HutD. Three conserved residues (Asp108, Asn110 and Arg61) in the pocket structure may be candidates for ligand binding sites.

Testing the hypothesis of HutD binding to urocanate: Thermal shift assay and ITC experiments were performed with purified HutD. The data suggest that HutD binds to urocanate but not histidine. However, the HutD-urocanate binding signal was very weak and detected at high urocanate concentration (53.23 mM), which is not physiologically relevant. Therefore, our current data does not support the hypothesis that HutD functions via binding to urocanate, the *hut* inducer.

Future work: The hypothesis that HutD binds to urocanate has not been completely rejected. The weak binding detected might be caused by photoisomerization of *trans*-UCA to *cis*-UCA, which was overlooked when the experiments were done. It is worthwhile to repeat the ITC experiment using pure *trans*-UCA.

Recent work by Dr Monica Gerth using ITC has shown that HutD from *P. aeruginosa* PAO1 binds to N-formylglutamate (FG) that is an inducer of HutG. If the hypothesis of HutD binding to urocanate is finally rejected, the ability of HutD binding to FG and other intermediates of the *hut* catabolic pathway should be tested.

References

Adams, M., & Jia, Z. C. (2005). Structural and biochemical analysis reveal pirins to possess quercetinase activity. *Journal of Biological Chemistry, 280*(31), 28675-28682.

Allison, S. L., & Phillips, A. T. (1990). Nucleotide sequence of the gene encoding the repressor for the histidine utilization genes of *Pseudomonas putida*. *Journal of Bacteriology, 172*(9), 5470-5476.

Amann, E., Ochs, B., & Abel, K. J. (1988). Tightly regulated *tac* promoter vectors useful for the expression of unfused and fused proteins in *Escherichia coli*. *Gene, 69*(2), 301-315.

Bailey, S. (1994). THE CCP4 suite - Programs for protein crystallography. *Acta Crystallographica Section D-Biological Crystallography, 50*, 760-763.

Bradford, M.M. (1976). A rapid and sensitive method for the quantitation of microgram quantities of protein utilizing the principle of protein-dye binding. *Anal. Biochem.* 72, 248-254.

Chasin, L. A., & Magasanik, B. (1968). Induction and Repression of the Histidine-degrading Enzymes of *Bacillus subtilis*. *Journal of Biological Chemistry, 243*(19), 5165-5178.

Davis, I. W., Leaver-Fay, A., Chen, V. B., Block, J. N., Kapral, G. J., Wang, X., Murray, L. W., Arendall, W. B., Snoeyink, J., Richardson, J. S., & Richardson, D. C. (2007). MolProbity: all-atom contacts and structure validation for proteins and nucleic acids. *Nucleic Acids Research, 35*, W375-W383.

Donovan, R. S., Robinson, C. W., & Glick, B. R. (1996). Review: Optimizing inducer and culture conditions for expression of foreign proteins under the control of the lac promoter. *Journal of Industrial Microbiology, 16*(3), 145-154.

Emsley, P., & Cowtan, K. (2004). Coot: model-building tools for molecular graphics. *Acta Crystallographica Section D-Biological Crystallography, 60*, 2126-2132.

Freyer, M. W., & Lewis, E. A. (2008). Isothermal titration calorimetry: Experimental design, data analysis, and probing Macromolecule/Ligand binding and kinetic interactions. In *Biophysical Tools for Biologists: Vol 1 in Vitro Techniques* (Vol. 84, pp. 79-113).

Gasteiger E., Hoogland C., Gattiker A., Duvaud S., Wilkins M.R., Appel R.D., *Bairoch A. (2005)*. Protein Identification and Analysis Tools on the ExPASy Server. In John M. Walker (Eds.), *The proteomics protocols handbook* (pp. 571-607). Humana Press.

Gouet, P., Courcelle, E., Stuart, D. I., & Metoz, F. (1999). ESPript: analysis of multiple sequence alignments in PostScript. *Bioinformatics, 15*(4), 305-308.

Holm, L., Kaariainen, S., Rosenstrom, P., & Schenkel, A. (2008). Searching protein structure databases with DaliLite v.3. *Bioinformatics, 24*(23), 2780-2781.

Hu, L., Mulfinger, L. M., & Phillips, A. T. (1987). Purification and properties of formylglutamate amidohydrolase from *Pseudomonas putida*. *Journal of Bacteriology, 169*(10), 4696-4702.

Hu, L., & Phillips, A. T. (1988). Organization and multiple regulation of histidine utilization genes in *Pseudomonas putida*. *Journal of Bacteriology, 170*(9), 4272-4279.

Hu, L., Allison, S. L., & Phillips, A. T. (1989). Identification of multiple repressor recognition sites in the *hut* system of *Pseudomonas putida*. *Journal of Bacteriology, 171*(8), 4189-4195.

Hug, D. H., & Hunter, J. K. (1994). Adventitious interconversion of *cis*-urocanic and *trans*-urocanic acid by laboratory light. *Photochemistry and Photobiology, 59*(3), 303-308.

Itoh, Y., Nishijyo, T., & Nakada, Y. (2007). Histidine catabolism and catabolite regulation. In J. L. Ramos & A. Filloux (Eds.), *Pseudomonas* (pp. 371-395). Dordrecht, Springer.

Kendrick, K. E., & Wheelis, M. L. (1982). Histidine Dissimilation in Streptomyces coelicolor. *J Gen Microbiol, 128*(9), 2029-2040.

Krissinel, E., & Henrick, K. (2004). Secondary-structure matching (SSM), a new tool for fast protein structure alignment in three dimensions. *Acta Crystallographica Section D, 60*(12 Part 1), 2256-2268.

Krissinel, E., & Henrick, K. (2007). Inference of macromolecular assemblies from crystalline state. *Journal of Molecular Biology, 372*(3), 774-797.

Laemmli, U. K. (1970). Cleavage of Structural Proteins during the Assembly of the Head of Bacteriophage T4. *Nature, 227*(5259), 680-685.

Landau, M., Mayrose, I., Rosenberg, Y., Glaser, F., Martz, E., Pupko, T., & Ben-Tal, N. (2005). ConSurf: the projection of evolutionary conservation scores of residues on protein structures. *Nucleic Acids Research, 33*, W299-W302.

Larkin, M. A., Blackshields, G., Brown, N. P., Chenna, R., McGettigan, P. A., McWilliam, H., Valentin, F., Wallace, I. M., Wilm, A., Lopez, R., Thompson, J. D., Gibson, T. J., & Higgins, D. G. (2007). Clustal W and Clustal X version 2.0. *Bioinformatics, 23*(21), 2947-2948.

Lo, M. C., Aulabaugh, A., Jin, G. X., Cowling, R., Bard, J., Malamas, M., & Ellestad, G. (2004). Evaluation of fluorescence-based thermal shift assays for hit identification in drug discovery. *Analytical Biochemistry, 332*(1), 153-159.

Lund, P., & Magasani.B. (1965). *N*-Formimino-L-glutamate formiminohydrolase of *Aerobacter aerogenes*. *Journal of Biological Chemistry, 240*(11), 4316-4319.

Magasanik, B. (1963). The genetic and molecular basis of catabolite repression. In H. Vogel, V. Bryson & J. O. Lampen (Eds.), *Informational macromolecules* (PP. 271-286). New York, Academic Press Inc.

Matthews, B. W. (1968). Solvent content of protein crystals. *Journal of Molecular Biology, 33*(2), 491-497.

McCoy, A. J., Grosse-Kunstleve, R. W., Adams, P. D., Winn, M. D., Storoni, L. C., & Read, R. J. (2007). Phaser crystallographic software. *Journal of Applied Crystallography, 40*, 658-674.

Mitraki, A., & King, J. (1989). Protein folding intermediates and inclusion body formation. *Bio-Technology, 7*(7), 690-697.

Moreland, N., Ashton, R., Baker, H. M., Ivanovic, I., Patterson, S., Arcus, V. L., Baker, E. N., & Lott, J. S. (2005). A flexible and economical medium-throughput strategy for protein production and crystallization. *Acta Crystallographica Section D, 61*(10), 1378-1385.

Murzin, A. G., Brenner, S. E., Hubbard, T., & Chothia, C. (1995). SCOP: a structural classification of proteins database for the investigation of sequences and structures. *Journal of Molecular Biology, 247*(4), 536-540.

Murshudov, G. N., Vagin, A. A., & Dodson, E. J. (1997). Refinement of Macromolecular Structures by the Maximum-Likelihood Method. *Acta Crystallographica Section D, 53*(3), 240-255.

Niesen, F. H., Berglund, H., & Vedadi, M. (2007). The use of differential scanning fluorimetry to detect ligand interactions that promote protein stability. *Nature Protocols, 2*(9), 2212-2221.

Orengo, C.A., Todd, A.E., & Thornton, J.M. (1999). From protein structure to function. *Curr. Opin. Struct. Biol., 9*(3), 374-382.

Otwinowski, Z., & Minor, W. (1997). Processing of X-ray diffraction data collected in oscillation mode. *Macromolecular Crystallography, Pt A, 276*, 307-326.

Pang, H., Bartlam, M., Zeng, Q. H., Miyatake, H., Hisano, T., Miki, K., Wong, L. L., Gao, G. F., & Rao, Z. H. (2004). Crystal structure of human pirin - An iron-binding nuclear protein and transcription cofactor. *Journal of Biological Chemistry, 279*(2), 1491-1498.

Pantoliano, M. W., Petrella, E. C., Kwasnoski, J. D., Lobanov, V. S., Myslik, J., Graf, E., Carver, T., Asel, E., Springer, B. A., Lane, P., & Salemme, F. R. (2001). High-density miniaturized thermal shift assays as a general strategy for drug discovery. *Journal of Biomolecular Screening, 6*(6), 429-440.

Stein, N. (2008). CHAINSAW: a program for mutating pdb files used as templates in molecular replacement. *Journal of Applied Crystallography, 41*(3), 641-643.

Thompson, I. P., Lilley, A. K., Ellis, R. J., Bramwell, P. A., & Bailey, M. J. (1995). Survival, Colonization and Dispersal of Genetically Modified *Pseudomonas fluorescens* SBW25 in the Phytosphere of Field Grown Sugar Beet. *Nat Biotech, 13*(12), 1493-1497.

Thornton, J.M., Todd, A.E., Milburn, D., Borkakoti, N. & Orengo, C.A (2000). From structure to function: approaches and limitations. *Nat. Struct. Biol., 7*, 991-994.

Zhang, X. X., George, A., Bailey, M. J., & Rainey, P. B. (2006). The histidine utilization (hut) genes of *Pseudomonas fluorescens* SBW25 are active on plant surfaces, but are not required for competitive colonization of sugar beet seedlings. *Microbiology, 152*, 1867-1875.

Zhang, C. & Kim, S.-H. (2003). Overview of structural genomics: from structure to function. *Curr. Opin. Chem. Biol. 7*(1), 28-32.

Zhang, X. X., & Rainey, P. B. (2007). Genetic analysis of the histidine utilization (*hut*) genes in *Pseudomonas fluorescens* SBW25. *Genetics, 176*, 2165-2176.

Zhang, X. X., & Rainey, P. B. (2008). Dual involvement of CbrAB and NtrBC in the regulation of histidine utilization in *Pseudomonas fluorescens* SBW25. *Genetics, 178*(1), 185-195.